International Journal of
Molecular Sciences

MDPI

Review

Advances in Monitoring Cell-Based Therapies with Magnetic Resonance Imaging: Future Perspectives

Ethel J. Ngen [1,*] and Dmitri Artemov [1,2]

[1] In Vivo Cellular and Molecular Imaging Center, Division of Cancer Imaging Research, Russell H. Morgan Department of Radiology and Radiological Sciences, Johns Hopkins University School of Medicine, Baltimore, MD 21205, USA; dartemo2@jhmi.edu

[2] Sidney Kimmel Comprehensive Cancer Center, Johns Hopkins University School of Medicine, Baltimore, MD 21205, USA

* Correspondence: engen1@jhmi.edu; Tel.: +1-410-502-8177

Academic Editor: Maurizio Muraca
Received: 26 October 2016; Accepted: 10 January 2017; Published: 19 January 2017

Abstract: Cell-based therapies are currently being developed for applications in both regenerative medicine and in oncology. Preclinical, translational, and clinical research on cell-based therapies will benefit tremendously from novel imaging approaches that enable the effective monitoring of the delivery, survival, migration, biodistribution, and integration of transplanted cells. Magnetic resonance imaging (MRI) offers several advantages over other imaging modalities for elucidating the fate of transplanted cells both preclinically and clinically. These advantages include the ability to image transplanted cells longitudinally at high spatial resolution without exposure to ionizing radiation, and the possibility to co-register anatomical structures with molecular processes and functional changes. However, since cellular MRI is still in its infancy, it currently faces a number of challenges, which provide avenues for future research and development. In this review, we describe the basic principle of cell-tracking with MRI; explain the different approaches currently used to monitor cell-based therapies; describe currently available MRI contrast generation mechanisms and strategies for monitoring transplanted cells; discuss some of the challenges in tracking transplanted cells; and suggest future research directions.

Keywords: cell-based therapies; cell-tracking; cellular MRI; MRI contrast agents; environmentally-responsive MRI biosensors

1. Introduction

Cell-based therapies are currently being developed and evaluated for applications in both regenerative medicine and in oncology [1–3]. There are currently 14,831 completed, and 8325 open on-going clinical trials on cell-based therapies throughout the world, registered on the United States National Institute of Health (NIH) clinical trials website [4,5]. Of these trials, ~68% of the completed trials (10,034) and ~71% of the open trials (5896) are related to cancer treatment [6,7].

In regenerative medicine, stem cell therapies enable the repair of damaged tissue either directly, by replacing injured cells in the tissue of interest, or indirectly, by paracrine signaling at the injury site, which stimulates the repair process [8–10]. Given the limited regenerative ability of the central nervous system (CNS), stem cell therapies are currently being investigated as potential solutions to a wide range of CNS-related disorders and injuries [11–13]. Applications for cell-based therapies in CNS regenerative medicine include: The reversal of neurodegeneration associated with diseases such as Alzheimer's disease, Parkinson's disease, amyotrophic lateral sclerosis (ALS), Huntington's disease, and demyelinating disorders, such as multiple sclerosis (MS) [12,14–22]. The reversal of the neurological deficits associated with spinal cord injuries, stroke, traumatic brain injuries, and brain

tumor therapy-related injuries, such as radiotherapy-induced brain injuries [23–35]. Stem cell therapies are also being investigated for wound-healing, and for the repair of damage to a variety of tissues, including cardiac, ocular, liver, bone, and cartilage tissue (Figure 1) [36–51].

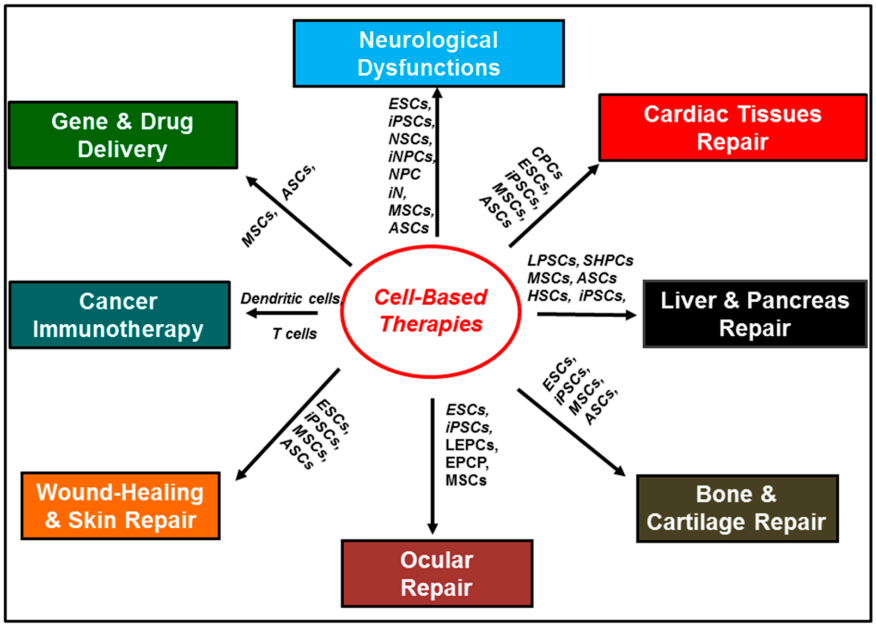

Figure 1. Schematic representing applications for cell-based therapies in regenerative medicine and in oncology. The following cell types are abbreviated in the figure: embryonic stem cells (ESCs); neural stem cells (NSCs); neural progenitor cells (NPCs); mesenchymal stem cells (MSCs); induced pluripotent stem cells (iPSC); induced neuronal cells (iN); induced neuronal progenitor cells (iNPCs); adipose-derived stem cells (ADSCs); embryonic germinal stem cells (EGC); endothelial progenitor cells (EPCs); cardiac progenitor cells (CPCs); lens epithelial progenitor cells (LEPCs); epithelial progenitor cells (EPCP); small hepatocytes-like progenitor cells (SHPCs); liver stem cells/progenitor cells (LPSCs); sinusoidal endothelial progenitor cells (SEPCs); hematopoietic stem cells (HSCs); and adipose stem cells (ASCs).

A variety of stem cells have been explored for both cell replacement therapies and to modulate physiological responses through paracrine action. Table 1 gives examples of the different types of stem cells that have been tested for various pathologies. Given the large number of preclinical studies that have been carried out, this table is not exhaustive but rather provides an overview.

Table 1. Examples of the different types of cells evaluated for various pathologies.

Disease Type	Examples of Cells Tested	Cell Therapy Rationale	References
Neurological Dysfunctions			
Parkinson's disease	Embryonic stem cells (ESCs); neural stem cells (NSCs); neural progenitor cells (NPCs); mesenchymal stem cells (MSCs); induced pluripotent stem cells (iPSC); induced neuronal cells (iN); induced neuronal progenitor cells (iNPCs).	Cell replacement therapy; immunomodulatory and neuroprotective properties	[11–17]
Alzheimer's disease	ESCs; NSCs; NPCs; MSCs; iPSCs; iN; iNPCs	Cell replacement therapy; immunomodulatory and neuroprotective properties	[12,18–20]
Huntington's disease	ESCs; NSC; NPC; MSC; adipose-derived stem cells (ADSCs).	Cell replacement therapy; immunomodulatory and neuroprotective properties	[12–14]

Table 1. *Cont.*

Disease Type	Examples of Cells Tested	Cell Therapy Rationale	References
Neurological Dysfunctions			
Amyotrophic lateral sclerosis	ESCs; NSCs; iPSCs; embryonic germinal stem cells (EGC)	Cell replacement therapy; immunomodulatory and neuroprotective properties	[12]
Multiple sclerosis	ESCs; iPSCs; MSCs; ADSCs;	Cell replacement therapy; immunomodulatory and neuroprotective properties	[20,21]
Central and Peripheral Nervous System (CNS and PNS) Injuries			
Spinal cord injuries	ESCs; MSCs; adipose-derived mesenchymal stem cells	Cell replacement therapy; neuroprotective properties.	[22–24]
Stroke	MSCs; ESCs; NSCs; iPSCs	Cell replacement therapy; immunomodulatory and neuroprotective properties.	[25–27]
Traumatic brain injuries	MSCs; iPSCs; bone-marrow-derived multipotent adult progenitor cells (MAPCs)	Cell replacement therapy; immunomodulatory and neuroprotective properties.	[28–30]
Radiotherapy-induced brain injuries	NSCs; ESCs; MSCs	Cell replacement therapy; immunomodulatory and neuroprotective properties.	[31–35]
Tissue Repair			
Skin (wound healing)	MSCs; ASCs; iPSCs; hematopoietic stem cells (HSCs); endothelial progenitor cells (EPCs)	Cell replacement therapy; paracrine action; modulation of physiological responses.	[36,37]
Heart	Cardiac progenitor cells (CPCs); MSCs; ASCs; iPSCs	Cell replacement therapy; paracrine action; modulation of physiological responses.	[38–40]
Eyes	Lens epithelial progenitor cells (LEPCs); epithelial progenitor cells (EPCP); inducible progenitor cells (iPSCs); MSCs.	Cell replacement therapy; paracrine action; modulation of physiological responses.	[41–44]
Liver	Small hepatocytes-like progenitor cells (SHPCs); Liver stem cells/progenitor cells LPSCs; Sinosoidal endothelial progenitor cells (SEPCs); Hematopoeitic Stem cells (HSCs); MSCs.	Cell replacement therapy; paracrine action; modulation of physiological responses.	[45,46]
Bone and cartilage	MSCs; ASCs.	Cell replacement therapy; paracrine action; modulation of physiological responses.	[47–51]
Cancer Immunotherapy			
Cancer	Dendritic cells; T cells	Stimulate immune response.	[52–57]
Drug and Gene Delivery			
Cancer	MSCs; ASCs.	Migratory properties.	[58–60]

In oncology, immune cells, such as dendritic cells, and natural and engineered T cells are being explored for cancer immunotherapy [52–57]. Given the migratory properties of stem cells in response to chemokines secreted in the tumor-microenvironment, stem cells such as mesenchymal stem cells, capable of phagocytosing therapeutic loads, are currently being explored as delivery vehicles for drugs, genes, and imaging agents [58–60]. Cell-based therapies are also currently used in the treatment of hematological malignancies, such as leukemia [61,62].

While cell-based therapies present potential solutions to a variety of problems in regenerative medicine and in oncology, preclinical research on these cell-based therapies and their translation to the clinic will benefit tremendously from imaging approaches that enable the noninvasive monitoring of the delivery, survival, migration, distribution, and integration of transplanted cells. This will permit the noninvasive assessment of the fate of transplanted cells longitudinally without the need for invasive biopsies and histological assessment, and enable the tailoring and personalization of cell-based therapeutic regimens.

2. Current Trends in Cellular Imaging

Several imaging modalities have been used to track transplanted cells both preclinically in small animal models and clinically in humans [63,64]. These include: optical imaging (fluorescence and bioluminescence imaging); nuclear imaging (positron emission tomography (PET) and single photon emission computed tomography (SPECT)); computed tomography; ultrasound imaging; and magnetic resonance imaging (MRI) (Figure 2). These modalities all have advantages, but also limitations for tracking transplanted cells. These advantages and limitations have been well documented in several recent review articles [63,64].

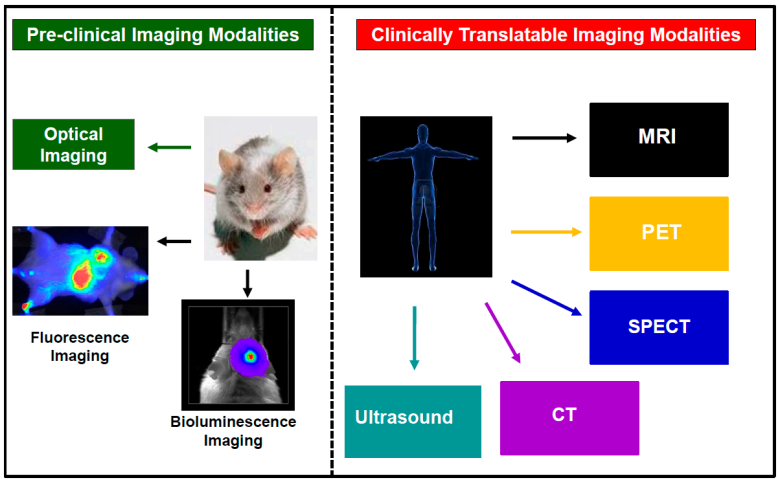

Figure 2. Schematic representing the different imaging modalities used in tracking cell-based therapies both preclinically and clinically. The following imaging modalities are abbreviated in the figure above: magnetic resonance imaging (MRI), positron emission tomography (PET); single photon emission computed tomography (SPECT); and computed tomography.

In this review, we focus on MRI as a tool for imaging transplanted cells. MRI has several advantages over other imaging modalities for tracking transplanted cells. A major advantage of MRI is that, unlike nuclear imaging which uses unstable radioactive isotopes as probes, with short lifetimes that generate ionizing radiation, MRI probes are not generated from radioactive isotopes, hence are stable and do not generate ionizing radiation. This permits the serial and longitudinal assessment of transplanted cells, at high spatial resolution without exposure to ionizing radiation [63,64]. Although, MRI is generally several orders of magnitude less sensitive than optical and nuclear imaging (detection limits of approximately 10^{-3}–10^{-5} M for MRI versus 10^{-9}–10^{-17} M for optical imaging and 10^{-10}–10^{-12} M for nuclear imaging) [63,64], it is possible to image single cells labeled with superparamagnetic iron oxide nanoparticles (SPIONs) in clinical 3T scanners, due to the "blooming" or magnetic susceptibility artifact, which causes the signal from the particles to extend beyond the immediate surroundings of the contrast agent, as a result of magnetic field inhomogeneities [65–67]. Thus, in combination with its high spatial resolution, MRI might be better suited than optical and nuclear imaging for tracking transplanted stem cells. There is currently a need for the development of MRI probes that permit the visualization of specific cellular and molecular processes.

3. The Principle of Cell Tracking with MRI

In order to track the delivery, migration, and survival of transplanted cells with MRI, it is imperative to endow the cells with MRI-sensitive properties via cell labeling, so that the cells can be detected after transplantation. Currently, three cell labeling techniques are generally used to endow cells with these properties: The direct cell labeling technique; the indirect cell labeling technique; and the encapsulation cell labeling technique (Figure 3).

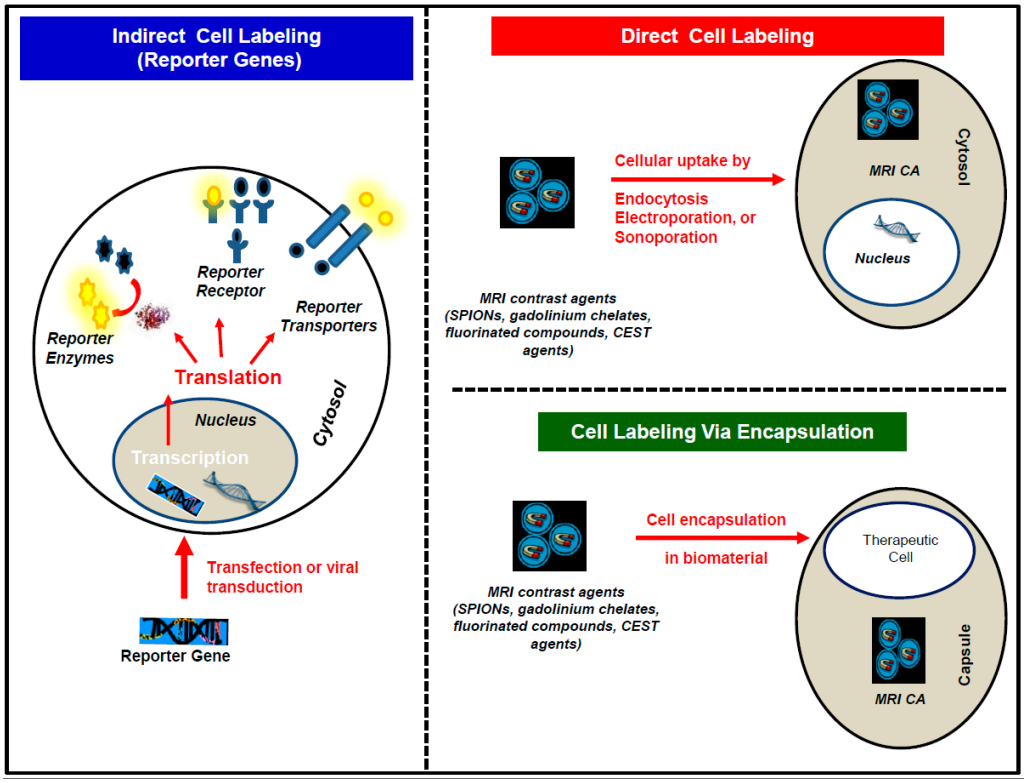

Figure 3. Schematic representing the different cell labeling approaches. Where, CA stands for contrast agents; CEST stands for chemical exchange saturation transfer; and SPIONs stands for superparamagnetic iron oxide nanoparticles.

3.1. The Direct Cell Labeling Technique

In the direct cell labeling technique, cells are incubated with an MRI contrast agent in vitro, and, prior to transplantation, usually with a transfection agent, such as poly-L-lysine (PLL) or lipofectamine [68–70]. The contrast agent is then endocytosed via either pinocytosis or phagocytosis, depending on its size. Other methods, such as electroporation and sonoporation have also been used to directly label cells with MRI contrast agents [71–73].

Although, the in vitro direct cell labeling technique is most often used to label cells prior to transplantation, several groups have demonstrated the feasibility of directly labeling endogenous cell populations in vivo, by targeting either the phagocytic nature of endogenous cell populations; or by targeting their cell surface receptors with either ligand or antibody-conjugated MRI contrast agents [74–79]. However, this in vivo direct cell labeling technique is usually used for either pathological diagnosis or to elucidate the role and the mechanism of action of endogenous cell populations in various pathologies [80,81]. Recently, in vivo labeling of cells prior to cell harvest and transplantation has been suggested [82,83]. However, this method is not generally used yet, to track transplanted cells. Several limitations of the in vivo cell labeling method have been identified. These include the following: This method will be limited to the labeling and harvesting of cells which are phagocytic in nature and easy to isolate, such as bone marrow-derived MSCs. For example, although it has been demonstrated that neural stem cells can be directly labeled in vivo, the difficulty of isolating these cells from the subventricular zone precludes the clinical application of this method for labeling and harvesting neural stem cells. This in vivo labeling approach will be most useful for allogeneic transplants, since in autologous transplants the patient would also have labeled phagocytic macrophages that would be difficult to distinguish from the transplanted MSCs. Additionally, since not all donors yield sufficient labeled stem cells for clinical dosing, the in vivo labeled cells harvested will have to be expanded prior to transplantation, and this could result in the serial dilution of the

MRI signal from the labeled cells to uncertain detection levels. More immune-phenotyping studies will also be required to ensure that the labeled cells harvested are indeed MSCs and not macrophages. Finally, this method does not provide a means to distinguish live transplanted cells from dead cells and could result in false-positive signals in the case of cell death, macrophage influx and secondary particle uptake. However, this method will still be clinically useful for tracking labeled cell transplantation in real-time using MR-compatible catheters and also for monitoring cell engraftment [83].

The exogenous direct cell labeling technique is currently the most employed cell labeling method, due to its simplicity and ease of use. However, it has a number of limitations. These include: The inability to effectively distinguish live labeled cells from dead labeled cells [84,85]. Since most MRI contrast agents such as SPIONs, paramagnetic gadolinium chelates, manganese-based nanoparticles, and perfluorocarbon nanoemulsions, all generate an MRI contrast whether in solution, within transplanted cells, or upon transfer of the contrast agent to infiltrating phagocytic immune cells such as macrophages, during graft rejection, it is usually difficult to distinguish live labeled cells from dead labeled cells [86,87]. Although several groups have suggested potential solutions for some MRI contrast generation mechanisms, this is still an area of active research and translational studies are still needed to standardize these proposed methods [88–91]. Examples of some of the proposed solutions for distinguishing live labeled cells from dead labeled cells include exploiting the differences in the transverse and longitudinal relaxation rates of T_2 and T_1 contrast agents respectively, when compartmentalized in live cell organelles compared to the relaxation rates of the free contrast agents when released from lysed dead cells [89,90,92]. Another proposed solution has been to exploit the effects of pH changes which usually accompany cell death, on the chemical exchange saturation transfer (CEST) rates of CEST contrast agents, to distinguish live cells from dead cells [93,94]. These examples and mechanisms are described in detail in Section 4 below. Another limitation of the exogenous direct cell labeling technique is the inability to reliably, serially quantify the proliferation and migration of labeled transplanted cells, due to the dilution of the MRI signal as the cells proliferate. Since a fixed amount of the contrast agent is present within the labeled cells after direct cell labeling, the MRI signal from the labeled transplanted cells decreases over time, as the contrast agent is distributed among the daughter cells during cell proliferation (contrast dilution) [90,95]. This renders precise cell quantification difficult.

3.2. The Indirect Cell Labeling Technique

In the indirect cell labeling technique, cells are either transiently transfected with the help of transfection agents or transduced with viral vectors to express an MRI reporter gene. An MRI reporter gene is a gene that can be either fused to a gene of interest or cloned instead of a gene of interest. Upon the expression of the MRI reporter gene as a peptide, protein nanostructure, receptor, enzyme, or cellular transporter it can either generate an inherent MRI contrast or interact via receptor binding, enzymatic activation or cellular efflux, with an administered MRI contrast agent to generate an MRI contrast.

Although, the indirect cell labeling technique is more complex than the direct cell labeling technique, it has several advantages over the direct cell labeling technique [63,64]. For example: Since the indirect cell labeling technique involves genetically engineering the cells to express the reporter gene of interest, the engineered cells proliferate to generate daughter cells that express the reporter gene of interest. Consequently, the MRI signal is not diluted as the cells proliferate [63,64]. Furthermore, live labeled cells can be reliably distinguished from dead labeled cells [86,87]. Since the labeled cells are genetically engineered to express the reporter gene of interest, the gene is expressed only in live cells and switched off in dead cells. This makes it possible to distinguish live cells from dead cells and accurately determine the survival of transplanted cells [63,64]. Recently, a study was carried out to evaluate the effectiveness of the direct cell labeling method using superparamagnetic iron oxide nanoparticles (SPIONs) compared to the indirect cell labeling method using genetically overexpressed ferritin (an iron storage protein). Briefly, mouse skeletal myoblasts were either labeled with SPIONs or

genetically engineered to overexpress ferritin. Along with the two live labeled cell transplant mouse groups, two other mouse groups received dead labeled cell transplants. In the two mice groups which received SPIONs labeled cells, live cells could not be distinguished from dead cells. However, in cells labeled with ferritin, only live cells were detected. Although ferritin was successful in distinguishing live cells from dead cells, the signal obtained from the ferritin labeled live cells was much lower compared to that obtained from the SPIONs labeled live cells [86].

Several other MRI reporter gene systems which use the different MRI contrast generation mechanisms have been developed [96,97]. Examples of MRI reporter gene systems that can be detected with the T_2/T_2* MRI contrast generation mechanisms include: the iron storage protein ferritin described above [98,99]; and the iron-binding receptor transferrin, responsible for cellular iron internalization [100]. However, these receptors and proteins all require the administration of exogenous T_2/T_2* MRI contrast agents such as SPIONs. The enzymes β-galactosidase which catalyzes the hydrolysis of β-D-galactosides is an example of a reporter gene that can be detected with the T_1 MRI contrast generation mechanism [101]. However, this system also requires the administration of exogenous T_1 contrast agents such as gadolinium chelates. Most recently, several reporter gene systems which use the CEST contrast generation mechanism and do not require the administration of exogenous contrast agents have also been developed. These include: the lysine rich protein (LRP); the super charged green fluorescent protein (ScGFP); human protamine-1 (hPRM-1) and the protein kinase A (PKA) sensor [102–105]. Other CEST MRI reporters which require the administration of exogenous CEST contrast agents have also been developed. These include the enzymes: herpes simplex virus type-1 thymidine kinase (HSV1-TK); and cytosine deaminase (CD) [106,107].

However, since the indirect cell labeling technique is still in its relative early stages of development, it still faces a few limitations that call for future research [97]. For example: In cases where an interaction with an MRI probe is needed to generate a signal, the use of imaging agents with unfavorable pharmacokinetic profiles could lead to a delayed MRI signal and consequently result in false-negative reporting. Additionally, since extremely high transduction efficiencies could impair the normal biological functioning of the engineered cells, transducing cells with optimal efficiencies to express the reporter gene of interest while still retaining the normal biological function could lead to low detection sensitivities, especially given the inherently low sensitivity of the currently available probes. Finally, a limitation that is often overlooked is that, since most of the currently developed genetically encoded reporters are of non-human origins (usually of bacterial origins), they are therefore immunogenic. While this might not pose a problem for the short-term (5–10 days) tracking of transplanted cells, the use of immunogenic reporters will limit their usefulness for longitudinal cell fate studies in the clinical setting. Thus, highly sensitive and non-immunogenic reporter genes and specific MRI probes with suitable pharmacokinetic profiles are needed for MRI.

3.3. The Encapsulation Cell Labeling Technique

Although the encapsulation technique has traditionally not been considered one of the cell labeling techniques, it has been included in this review due to its growing use. In the encapsulation cell labeling technique, biomaterials such as alginate capsules are used to protect therapeutic cells from infiltrating immune cells. Alginate is a biocompatible polymer, purified from algae, that has been extensively used for cell encapsulation [108,109]. These alginate capsules permit the diffusion of low molecular weight compounds, thus are permeable to small molecules such as water and nutrients but impermeable to infiltrating immune cells. Polycations such as poly-L-lysine (PLL) have been used extensively to control the pore sizes (permeability) of the capsules and also to provide stability for the capsules [108,109]. Generally, these capsules are approximately 350 μm in diameter and can hold varying numbers of single cells depending on the cell size [110]. For human islet cells, one islet is generally used per capsule [109]. However, for single cells such as MSCs, up to 300 MSCs can be enclosed in a single capsules, and up to 500 capsules can be administered [108,109]. Both the therapeutic cells and the MRI

contrast agents are encapsulated together in vitro, prior to transplantation [108–112]. The MRI contrast agent then generates a signal that reports on the status of the transplanted cells.

While this method can be used to report on the delivery and survival of transplanted cells, it is not designed to report on cell migration or integration.

4. MRI Contrast Generation Mechanisms

Several MRI contrast agents that function through different contrast generation mechanisms have been developed and used to track transplanted cells. These include: Agents that affect the transverse relaxation rates (R_2/R_2*) of water protons in their surroundings (T_2/T_2* agents); agents that affect the longitudinal relaxation rates (R_1) of water protons in their surroundings (T_1 agents); agents with exchangeable protons or coordinated water molecules that can be saturated with specific radiofrequency pulses, and that can transfer the saturation to surrounding non-saturated water protons or molecules via chemical exchange saturation transfer (CEST agents); and agents that possesses NMR-detectable nuclei not typically found in biological systems, such as fluorine (^{19}F), which can generate MRI "hot spots". These agents all have advantages for tracking transplanted cells, but also limitations, which provide avenues for future research and development.

4.1. T_2/T_2 Contrast Agents*

T_2/T_2* contrast agents are currently the most widely used MRI contrast agents for tracking transplanted cells both preclinically and clinically [113–115]. T_2/T_2* agents function by decreasing the transverse relaxation rates (R_2/R_2*) of water protons in their surroundings, predominantly via perturbation of the magnetic field homogeneity, and have a lesser effect on the longitudinal relaxation rates (R_1) of water protons [116,117]. Since the perturbation of the magnetic field homogeneity by these agents results in the loss of the MRI water signal, their presence is identified on MR images by a signal void or darkening (hypointensity) of their local surroundings [116,117]. However, this signal void could also result from other sources such as chemical shift artifacts, hemorrhage, and air bubbles and could lead to a misinterpretation of the images. This false-positive misinterpretation is generally not encountered with the other MRI contrast agents which generate positive contrast such as T_1 agents and fluorine "hot spot" agents [118].

Although the most widely used T_2/T_2* MRI contrast agents in preclinical studies and in clinical trials are superparamagnetic iron oxide nanoparticles (SPIONs) [119,120], there are currently no T_2/T_2* MRI contrast agents FDA-approved for tracking transplanted cells. However, clinical grade SPIONs, FDA-approved for other applications have been employed in several cell-tracking clinical trials [113]. Clinical grade SPIONs, FDA-approved for liver imaging that have been used in clinical trials for tracking transplanted cells include: an SPION with a dextran coating called Endorem® in Europe and Feridex® in the USA; and an SPION with a carboxydextran coating called Resovist® [113,121,122]. However, the production of Feridex® was discontinued in 2009, due to commercial considerations, since there was little demand for its FDA-approved application [113]. Feromuxytol, an ultra-small superparamagnetic iron oxide nanoparticle (USPION), FDA-approved for the treatment of iron deficiencies in patients with renal failure [123], has also been suggested for tracking stem cells [124]. However, USPIONs (~5 nm in diameter) are generally less sensitive than SPIONs (~80–150 nm in diameter) for tracking transplanted cells. Thus, developing clinical grade SPIO-based MRI contrast agents for tracking transplanted cells is an area of active research. This includes developing agents with large SPIO cores and biocompatible polymer surfaces, such as poly lactic-co-glycolic acid (PLGA), an FDA-approved polymer for drug delivery [125–127].

There is also a need for the development of nanoparticles with different degradation kinetics and subsequently different lifetimes, which could be used for different cell tracking purposes. For example, since immune cells have short lifespans, monitoring immune cells will be better achieved with particles with faster degradation kinetics. This would prevent the persistence of the particles long after the immune cells have died, and prevent the detection of false-positive signals [128]. Imaging stem cells,

which have much longer lifespans, would however, require particles with longer lifetimes. In a particle degradation kinetics study, it was demonstrated that the rate of particle degradation was affected primarily by the particle surface coating and secondarily by the particle size [128]. The rate of particle degradation was faster in particles coated with more biodegradable polymers such as PLGA than in particles coated with cellulose. In PLGA particles, the rate of degradation was faster in PLGA-coated nanoparticles than in PLGA-coated microparticles. This is expected, since PLGA nanoparticles were initially designed for drug delivery and degradation of the particles to release the drug load was key to the success of these particles [126]. While the degradation of these particles and their ability to track MSCs has been demonstrated in vivo [125], the use of these particles to track transplanted immune cells in vivo short-term still needs to be demonstrated.

T_2/T_2^* MRI agents function predominantly by perturbing the magnetic field homogeneity in their local surroundings, and this perturbation is greater with particles of larger iron core sizes that possess larger magnetic moments [66,129]. Thus, several strategies have been developed, based on this principle to improve the sensitivity of T_2/T_2^* agents. These include developing micron-sized particles that possess larger SPIO cores [130,131]. Genetically encoded reporters have also been developed, which produce iron-binding proteins such as ferritin, an iron storage protein, which can bind to iron endogenously present in the organism and thus increase the intracellular iron concentration or bind to administered iron oxide nanoparticles, to form MRI-sensitive large iron aggregates [99,132–134]. This strategy was used to distinguish live mouse skeletal myoblasts genetically engineered to express ferritin from dead genetically engineered cells transplanted to the mouse heart [86].

While labeling cells with T_2/T_2^*-genetically encoded reporters can be used to track cell delivery, migration, survival and differentiation, SPIO-based T_2/T_2^* MRI agents are most effective in tracking cell delivery and migration, but are difficult to use in tracking cell survival and differentiation [86,87,135]. Thus, several strategies for predicting cell survival with SPIO-based T_2/T_2^* MRI agents have been developed [88–90,92,95,136–138]. These strategies exploit molecular and cellular differences between live and dead cells in modulating changes in the relaxivity. These molecular and cellular differences include differences in: cell membrane permeability, enzymatic activity, pH, and proliferation rates [139,140].

A particularly promising, yet simple approach called the MRI dual contrast technique was recently developed to detect cell death of transplanted SPION-labeled cells in real time [88]. This MRI dual contrast method involves labeling cells with both a high molecular weight (low diffusion coefficient) T_2/T_2^* agent such as SPIONs and a low molecular weight (high diffusion coefficient) T_1 agent, such as gadolinium-based chelates [88,141,142]. In live cells, where the cell membrane is intact and both contrast agents are in close proximity to each other, the T_2/T_2^* signal from the SPIONs predominate and mask the T_1 signal from the T_1 agent (Figure 4). This T_2/T_2^* signal from the SPIONs can then be used to track cell delivery and migration (Figure 4b). However, in the case where the cells die after transplantation (in immune-competent mice), the cell membrane is disrupted, and both contrast agents are released from the dead cells. The T_1 agent with a high diffusion coefficient diffuses away from the SPION with a low diffusion coefficient and generates a T_1 signal, in the vicinity of the T_2/T_2^* signal (Figure 4c–f). This T_1 signal is then used to indicate cell death. Both the T_2/T_2^* signal and the T_1 signal can be separated using a spin echo pulse sequence and appropriate acquisition parameters, when both contrast agents are as little as ~15 μm away from each other [88,141,142]. This dual contrast cell labeling technique was used to track MSCs transplanted to repair radiation-induced brain injury (RIBI) in a mouse model (Figure 4). However, the dual contrast cell labeling technique could also be applied to monitor other types of stem cells such as NSCs, transplanted to repair traumatic brain injury or even stroke, clinically.

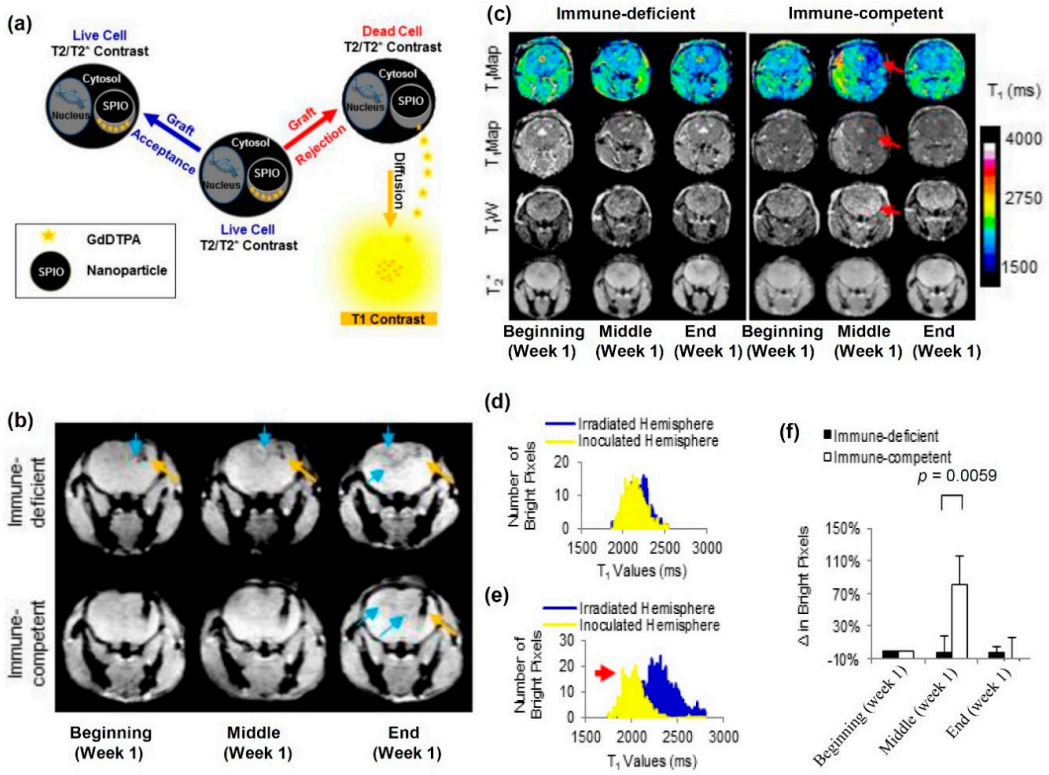

Figure 4. Cell tracking using the MRI dual contrast technique. (**a**) Schematic representing live cell-tracking by T_2/T_2* contrast enhancement, and cell death detection by T_1 contrast enhancement. Where SPIO stands for superparamagnetic iron oxide and GdDTPA stands for gadolinium-diethylenetriaminepentaacetic acid. (**b**) T_2*-weighted images of immune-deficient and immune-competent mouse brains, indicating the site of cell delivery (↑) and cell migration to the radiation-induced lesion (↑). More cell migration to the injury site was detected in immune-deficient mice; (**c**) Comparison of T_1 contrast enhancement in immune-deficient and immune-competent mice, respectively, within the first week of cell transplantation. A significant T_1 contrast enhancement was observed in the slice adjacent to that of the cell delivery site in immune-competent mice. (↑) represents T_1 contrast enhancement in the slice adjacent to that of cell delivery; (**d**) Pixel intensity histograms of the ipsilateral and contralateral hemispheres of cell implantation before graft rejection indicate similar T_1 values in both hemispheres; (**e**) Pixel intensity histograms of the ipsilateral and contralateral hemispheres of cell implantation after graft rejection indicate lower T_1 values in the hemispheres ipsilateral to cell implantation. (↑) represents T_1 contrast enhancement in the slice adjacent to that of cell delivery; (**f**) Quantification of T_1 contrast enhancement in immune-deficient and immune-competent mice, respectively, at the beginning, middle, and end of week one. The signals were normalized for each mouse and indicate significant T_1 contrast enhancement within week one in immune-competent mice, indicating cell death. The images and caption are reprinted from Ngen et al. [88].

While this environmentally-responsive SPIO-based T_2/T_2* nanosystem and others proposed are promising, this is still an area of active research. These nanosystems and acquisition methods still need to be optimized and validated before they can be clinically translated. For example, given the rapid clearance of low molecular weight gadolinium chelates after they are released from dual labeled dead cells, the imaging schedule is very important in obtaining accurate readings. Thus, for this method to be clinically translated, a more standardized imaging schedule will need to be defined. Additionally, given the intrinsically lower sensitivity of MRI to detect low molecular weight gadolinium chelates compared to SPIONs, this method is currently most suitable for the detection of hyper acute and acute cell death, where high concentrations of the gadolinium chelates are released instantaneously from a large number of dead cells, and can be detected with MRI (detection limit within the micromolar

concentration range). Thus, for this nanosystem to be applied universally for detecting cell death, gadolinium chelates with slower clearance rates, compatible with standardized imaging schedules will be needed. Finally, since this method relies on the diffusion of low molecular weight gadolinium chelates through breached cell membranes to detect cell death, and also since low molecular weight gadolinium chelates (<800 Da) are sufficiently small (<2 nm in diameter) to diffuse through apoptotic pores generated during apoptosis, this method is not designed to distinguish between apoptotic versus necrotic cell death mechanisms. For this method to detect specific cell death mechanisms, probes based on the dual contrast technique and capable of sensing biomarkers associated with specific cell death mechanisms such as enzymatic expression, will be needed.

4.2. T_1 Contrast Agents

T_1 contrast agents function by reducing the longitudinal relaxation rate (R_1) of water protons in the surroundings of the agents. This leads to a gain in the MRI signal and results in a brightening of the voxels with high concentrations of the agents on T_1-weighted MR images [116,117].

Traditionally, T_1 MRI contrast agents that have been used to track transplanted cells have been paramagnetic gadolinium-based and manganese-based agents [143–145]. However, T_1 MRI contrast agents are less often used in tracking cell-based therapies than T_2/T_2* agents, due to their lower sensitivity. Several nanotechnology strategies have thus been developed to overcome this limitation. These include developing nanoparticles and liposomes with large clusters of the paramagnetic agents to enhance the sensitivity of the agents [146–149]. However, T_1 agents require direct contact with the surrounding water protons to modulate the contrast as opposed to T_2/T_2*, which do not require direct contact with the surrounding water protons, but can disrupt the local magnetic field homogeneity in the vicinity of the magnetic nanoparticle and modulate the contrast [116,117]. Thus, mesoporous nanoparticles (usually silica-based nanoparticles doped with the paramagnetic agents) that enable the direct contact of the paramagnetic agents in the nanoparticles with surrounding water protons have been developed [143,145,146].

Another challenge in using T_1 MRI contrast agents is the possibility of quenching the T_1 relaxation, depending on the cellular localization and concentration of the agent. In cases where high concentrations of the agents are sequestered in the lysosomes of the cells, with limited water accessibility, this could lead to a quenching of the T_1 relaxation [150,151]. Thus, cell labeling techniques that enable the cytosolic localization of the agents at appropriate concentrations, such as electroporation and sonoporation, have also been investigated [150,151].

Although, gadolinium-based and manganese-based T_1 contrast agents have been used to monitor cell delivery and migration; monitoring cell survival and differentiation has been a challenge [63,64]. Several strategies that modulate the relaxivity by exploiting the molecular and cellular differences between live and dead cells have been developed [90,152,153]. This is an ongoing area of research [140,154]. An example which exploits the differences in the cell membrane permeability between live and dead cells in modulating changes in longitudinal relaxation rates (R_1) has been used to distinguish live cells labeled with gadolinium chelates from dead labeled cells [90]. It was shown that the differences in the longitudinal relaxation rates of gadolinium chelates in live transplanted cells, where the agents are entrapped by the cell membrane and have limited water accessibility, differ from that of gadolinium chelates in dead cells, were the cell membranes are disrupted and the agents have more water accessibility.

Another interesting approach was recently developed which exploits the expression of the caspase-3 enzyme (an apoptosis biomarker), to distinguish live cells from apoptotic cells, using a gadolinium-based caspase-3 activable probe (Figure 5) [152]. In this method called caspase-3-sensitive nanoaggregation MRI (C-SNAM), the probe self-assembles into nanoparticles after hydrolysis by caspase-3, released from apoptotic cells. This aggregation leads to an enhancement of the relaxivity and prolongs in vivo retention of the probe. Although, this method does not involve labeling the cells with the probe prior to transplantation, but rather depends on administering the probe locally at the

transplantation site, it is a good example of tracking cell survival using environmentally-responsive T_1 agents.

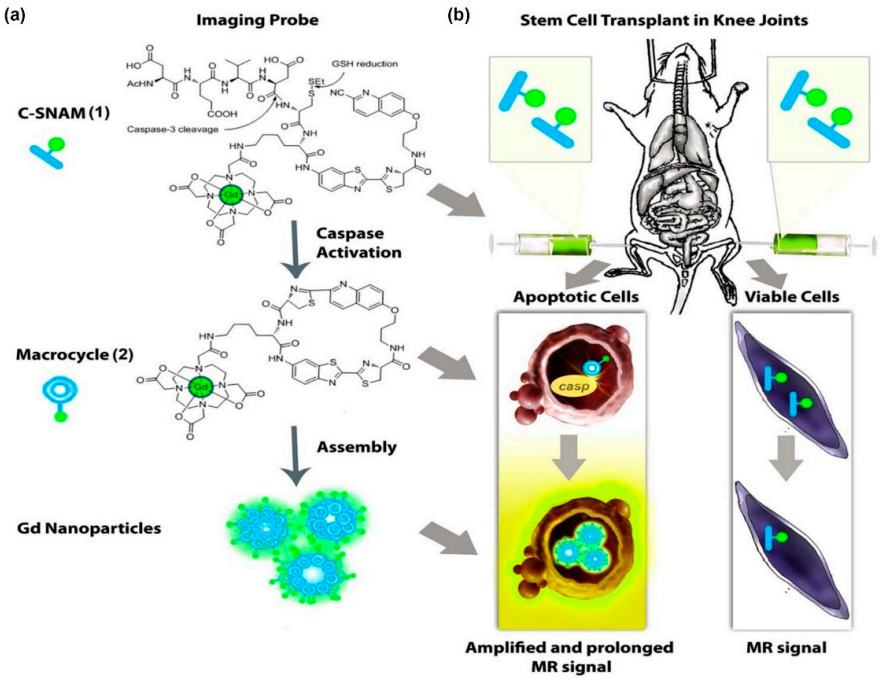

Figure 5. General design and mechanism of action of the caspase-3-sensitive nanoaggregation MRI probe (C-SNAM). (**a**) Chemical structure of C-SNAM. Following disulfide reduction and caspase-3-triggered DEVD peptide cleavage, C-SNAM transforms to a rigid and hydrophobic macrocyclic product 2, through a biocompatible intramolecular cyclization reaction between 2-cyano-6-hydroxyquinoline and D-cysteine residue. The macrocycle 2 will subsequently self-assemble into Gd nanoparticles, leading to an increase in longitudinal relaxivity (r_1) relative to the unactivated probe 1; (**b**) Corresponding mechanism of action in vivo. (1) Intra-articular injection of C-SNAM into rat knee joints with implants of apoptotic and viable stem cells. (2) In vivo activation of C-SNAM in apoptotic stem cell transplants through caspase-3-mediated activation. (3) Increased relaxivity and retention effect of GdNPs lead to enhanced MRI signal of apoptotic stem cell transplants. The images and caption are reprinted with permission from Nejadnik et al. [152].

Several reporter gene systems that could be used to monitor gene expression in transplanted cells using activable T_1 contrast agents have also been developed, such as the *lacZ* gene which encodes the enzymes β-galactosidase that catalyzes the hydrolysis of β-D-galactosides [101,155,156]. However, the extensive use of these systems has been limited due to their low sensitivity in vivo. Given the nephrotoxicity associated with gadolinium-based contrast agents, several non-metallic biosensors based on the chemical exchange saturation transfer contrast mechanism and fluorine MRI, described in Sections 4.3 and 4.4 below, are currently being explored as alternatives [157–159].

4.3. Chemical Exchange Saturation Transfer (CEST) Contrast Agents

CEST contrast agents are a relatively new class of MRI contrast agents. These agents generate an MRI contrast by reducing the signal from water protons in their surroundings, following chemical exchange and saturation transfer from protons on the contrast agent or water molecules coordinated to the contrast agent and selectively saturated with an appropriate radiofrequency pulse, to water protons or free water molecules in their surroundings [160].

There are two main classes of CEST contrast agents: diamagnetic and paramagnetic CEST agents [161]. Generally, diamagnetic CEST (DIACEST) contrast agents are organic molecules with

exchangeable protons such as amine, amide, and hydroxyl protons that can undergo chemical exchange and saturation transfer with the surrounding water protons, following selective saturation of the protons of interest. Since these agents are not metal-based, the toxicity associated with metal-based MRI contrast agents is avoided with their usage [159].

Paramagnetic CEST contrast agents (PARACEST), however, are usually chelates of paramagnetic lanthanide ions (metal-based). These agents generate contrast by reducing the signal from water protons in their surroundings, following the chemical exchange and saturation transfer of selectively saturated water molecules coordinated (bound) to the contrast agents with non-coordinated (unbound) free water molecules. PARACEST agents generate less background signal than DIACEST agents, due to the large chemical shift difference between the saturated coordinated water molecules of interest and the free water molecules. Both types of agents have been used to monitor transplanted cells [93,162]. Recently, PARACEST agents (europium and ytterbium chelates) were used to monitor tissue engineering by NSCs and endothelial cells within a stroke cavity in a preclinical rodent stroke model. The distribution of the different cell types within the lesion cavity and the individual contribution of the different cell types to morphogenesis were successfully monitored simultaneously using both PARACEST agents. This study demonstrated the importance of imaging agents to guide the delivery of the different cellular building blocks for de novo tissue engineering and to understand the dynamics of cellular interactions in de novo tissue formation [162].

Given the sensitivity of chemical exchange rates and chemical shifts to environmental factors such as pH and ionic strength and content, which are in turn affected by cell physiological conditions, CEST agents have been used as environmentally-responsive MRI biosensors to monitor cell viability [129,139]. An L-arginine liposome with multiple exchangeable amine protons was developed as a pH-sensitive DIACEST nanosensor to monitor cell death of encapsulated cells in vivo (Figure 6) [93]. This method exploits the sensitivity of the exchange rate of the guanidyl protons of L-arginine to pH changes in the range typically associated with the cell death process (pH 7.4–6.0). In live cells, where the pH is close to 7.4, the exchange rate between the saturated guanidyl protons of the L-arginine liposome and those of the surrounding bulk water protons is optimal. However, in apoptotic cells where the pH drops from pH 7.4 to about pH 6.0, the exchange rate decreases and subsequently the CEST signal also decreases. This decrease in the CEST contrast is then used to indicate cell death.

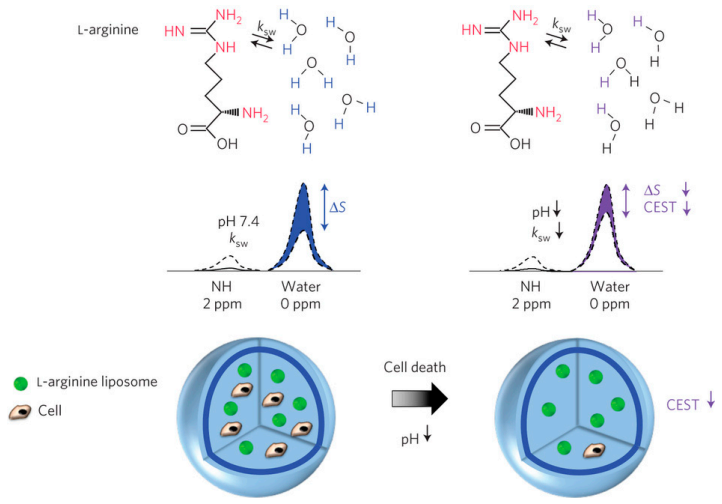

Figure 6. Schematic representing the principles of in vivo detection of cell viability using LipoCEST microcapsules as pH nanosensors. The CEST contrast is measured by the drop in the signal intensity (ΔS) of water after selective saturation (that is, removal of capability to generate signal) of the NH protons in L-arginine at 2 ppm. The L-arginine protons (red) inside the LipoCEST capsules exchange saturation (ksw) with the surrounding water protons. The ksw is reduced at lower pH causing a significant drop in CEST contrast. The images are reprinted with permission from Chan et al. [93].

Genetically encoded CEST reporters have also been developed, which could enable the monitoring of transplanted cells [102–104,106]. Although these systems have been tested for cancer detection, their application in regenerative medicine still needs to be demonstrated. Examples of CEST genetically-encoded reporters include CEST-responsive peptides such as: the lysine rich protein (LRP); the super charged green fluorescent protein (ScGFP); human protamine-1 (hPRM-1) and the protein kinase A (PKA) sensor, which do not require the administration of exogenous contrast agents, [102–105]. Other CEST MRI reporters which require the administration of exogenous CEST contrast agents have also been developed. These include the enzymes: herpes simplex virus type-1 thymidine kinase (HSV1-TK); and cytosine deaminase (CD) [106,107]. However, the main limitation of these agents has been their relatively lower sensitivity compared to T_2/T_2^* agents. This could affect the detection of transplanted cells in regenerative medicine where generally fewer cells per voxel need to be detected compared to tumor masses. Thus, developing more sensitive, non-immunogenic, genetically encoded reporters is an active area of research [163].

A third class of CEST contrast agents (hyperCEST agents), have very recently been developed. These agents exploit transfer between protein-bound hyperpolarized xenon (^{129}Xe) and unbound hyperpolarized ^{129}Xe [163,164]. The hyperCEST technique makes use of xenon-binding structures, such as cryptophanes, which induce large chemical shifts of ^{129}Xe, between bound and unbound states [165–167]. Since these agents involve the use of hyperpolarized nuclei, they are more sensitive than other MRI agents [165,168]. However, the short lifetime of hyperpolarized ^{129}Xe in vivo limits their extensive application.

4.4. Fluorine (^{19}F) Contrast Agents

The fluorine-19 isotope (^{19}F) is a stable NMR-detectable nuclei, which can be used in MRI, unlike the radioactive fluorine-18 isotope (^{18}F) used in PET. ^{19}F MRI has been used to track the delivery and migration of transplanted cells [70,169–171]. Since fluorine is not naturally found in biological systems, there is no background signal from the tissue when these agents are used. Given the relatively low sensitivity of ^{19}F MRI, most systems used to track transplanted cells have been based on nanocarriers, such as perfluorocarbon-based (PFC) and perfluoropolyether (PFPE) nanoemulsions, which can hold several ^{19}F atoms [172,173]. Dendritic cells which are being explored as immunotherapies for cancer and autoimmune diseases have been successfully labeled with PFPE. An intracellular concentration of 5.2×10^{12} fluorine spins or 0.25 ng of PFPE was determined by ^{19}F NMR. The cells were then injected to mice either intravenously into tissue and monitored with ^{19}F MRI, using an 11.7 T preclinical animal scanner. The anatomical location of the cells was determined by proton (^{1}H) MRI.

There has been great enthusiasm for the use of PFC nanoemulsions in clinic due to their relatively low toxicity, their exceptionally high cell specificity and the possibility of cell quantification in vivo. However, one of the main challenges to the clinical translation of ^{19}F MRI for tracking immune cells is the development of appropriate hardware sufficiently robust to image large areas of the human body [174,175]. Current methods to image immune cells rely on acquiring two sets of images: ^{19}F MRI which gives information on the transplanted cells and ^{1}H MRI which gives anatomical information that helps locate the cells. However, the image co-registration between the acquisitioning of the two nuclei images could vary due to the coil handling and/or subject motion. Secondly, the sensitivity of the images acquired from the different nuclei could differ. Thus, several efforts for the clinical translation of ^{19}F MRI are focused on the development of dual radiofrequency (RF) coils capable of simultaneously acquiring ^{1}H and ^{19}F MRI in large subjects.

Recently, formulations of PFPE nanoemulsions with improved sensitivity for cellular MR were also developed [173]. These constructs consisted of metal-binding β-diketones conjugated to linear PFPE. These fluorinated ligands were formulated as aqueous nanoemulsions and then metallated with various transition and lanthanide ions in the fluorous phase (Figure 7a). The iron (III) tris-β-diketonate (FETRIS) nanoemulsions, showed superior MRI properties and low cytotoxicity. The resulting ^{19}F MRI signal was enhanced by three-to-five-fold over previously used tracers at 11.7 T, (Figure 7).

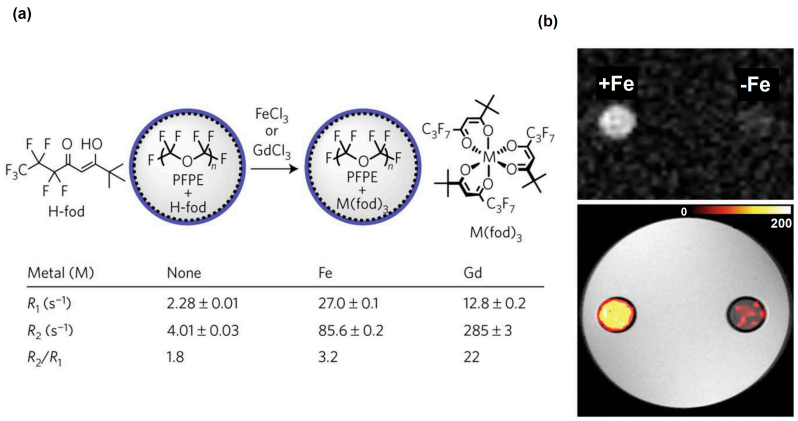

Metal (M)	None	Fe	Gd
R_1 (s^{-1})	2.28 ± 0.01	27.0 ± 0.1	12.8 ± 0.2
R_2 (s^{-1})	4.01 ± 0.03	85.6 ± 0.2	285 ± 3
R_2/R_1	1.8	3.2	22

Figure 7. (**a**) Comparison of iron and gadolinium diketonates (H-fod) as ^{19}F relaxation agents for PFPE. The relaxometry results (9.4 T) are shown for PFPE emulsions (120 g l^{-1} PFPE) containing H-fod (2.8 mM) 24 h after the addition of 0.7 mM metal ions. R_1, spin–lattice relaxation rate (=1/T_1), and R_2, spin–spin relaxation rate (=1/T_2), values are reported for the main PFPE peak at −91.4 ppm. The results show that Fe^{3+} is a more effective R_1 agent than Gd^{3+}. (**b**) MRI of FETRIS nanoemulsion. Phantom comprised of two agarose-embedded NMR tubes containing FETRIS nanoemulsion (4.5 g·L^{-1} ^{19}F) with 0.5 mM Fe^{3+} (R_1/R_2 = 32.5/170 s^{-1}) and nanoemulsion without metal (R_1/R_2 = 2.2/3.7 s^{-1}), denoted +Fe and −Fe, respectively. The top panel shows unthresholded ^{19}F images, and below, the ^{19}F image is thresholded, rendered in hot-iron pseudo-color (scale bar), and overlaid onto the greyscale ^{1}H image. The ^{19}F/^{1}H MRI data were acquired using a gradient echo (GRE) sequence. The images and caption are reprinted with permission from Kislukhin et al. [173].

While ^{19}F MRI has been used to track cell delivery and migration, tracking the functional status (survival and differentiation) of transplanted cells with these ^{19}F nanosystems has been a challenge. Thus, future directions in this field will focus on developing environmentally-responsive ^{19}F nanosystems capable of reporting on the functional status of transplanted cells. Several ^{19}F systems, capable of sensing the presence of metal ions in their micro-environment such as zinc and iron, have been developed [176–178]. Since metal ions, such as zinc and iron ions, play a fundamental role in the functioning of cells, these systems could be developed to report on the functional status of transplanted cells. However, more research in preclinical models is still needed on these systems before they can be translated clinically.

Genetically encoded ^{19}F reporters capable of reporting on the activity of transplanted cells have also been developed [179–181]. The feasibility of monitoring the expression and activity of β-galactosidase, the product of the *lacZ* gene, in transfected cells was demonstrated using ^{19}F NMR chemical shift imaging (CSI), using different prototype reporter molecules [179–181]. However, like other reporter gene systems, for these systems to be translated to clinic, the regulatory hurdles associated with genetic engineering still need to be addressed. Additionally, the hardware limitations associated with imaging large subjects, discussed above, also need to be addressed.

5. Conclusions

Although cellular MRI is still in its infancy, several promising cellular MRI techniques have been developed to monitor the delivery, migration, and biodistribution of the transplanted cells. However, monitoring the functional states of transplanted cells, including their survival and differentiation, is still a challenge. Thus, future research in cellular MRI is bound to focus on the development and translation of environmentally-responsive MRI contrast agents, capable of reporting on the status of transplanted cells. Several strategies that exploit molecular and cellular differences between live and dead cells in modulating changes in relaxivity and chemical exchange rates are currently being explored for the development of environmentally-responsive MRI agents. These differences include differences

in cell membrane permeability, enzymatic activity, and pH. The clinical translation of cell-based therapies would benefit tremendously from the development of more robust and sensitive probes with better pharmacokinetic profiles, which will permit the effective detection of specific cellular processes associated with cell death and differentiation at high spatial and temporal resolutions. This could accelerate the clinical translation and personalization of cell-based therapies.

Acknowledgments: The authors would like to thank Ms. Mary McAllister for editing this manuscript. This research was sponsored by the TEDCO Maryland Stem Cell Research Fund (2010-MSCRFE-0096) and the American Brain Tumor Association (ABTA) Basic Research Fellowship in honor of Joel A. Gringas (grant number: 117704).

Author Contributions: Ethel J. Ngen designed and drafted the manuscript. Dmitri Artemov revised the manuscript.

Conflicts of Interest: The authors declare no competing financial interests.

Abbreviations

ADSCs	Adipose-derived stem cells
ALS	Amyotrophic lateral sclerosis
CEST	Chemical exchange saturation transfer
CNS	Central nervous system
CPCs	Cardiac progenitor cells
CT	Computed tomography
DIACEST	Diamagnetic chemical exchange saturation transfer
EGCs	Embryonic germinal cells
EPCs	Epithelial progenitor cells
ESCs	Embryonic stem cells
FDA	Food and drug administration
^{18}F	Fluorine-18 isotope
^{19}F	Fluorine-19 isotope
HSCs	Hematopoietic stem cells
HyperCEST	Hyperpolarized chemical exchange saturation transfer
iN	Induced neuronal cells
iNPCs	Induced neuronal progeneitor cells
iPSCs	Induced pluripotent stem cells
LEPCs	Lens epithelial progenitor cells
LPSCs	Liver stem cells/progenitor cells
MRI	Magnetic Resonance Imaging
MS	Multiple sclerosis
MSCs	Mesenchymal stem cells
NIH	National Institute of Health
NPCs	Neural progenitor cells
NSCs	Neural stem cells
PARACEST	Paramagnetic chemical exchange saturation transfer
PET	Positron emission tomography
pH	Hydrogen potential
PLGA	Poly lactic-co-glycolic acid
PLL	Poly-L-lysine
R_1	Longitudinal relaxation rate
R_2	Transverse relaxation rate
SEPCs	Sinosoidal endothelial progenitor cells
SHPCs	Small hepatocytes-like progenitor cells
SPECT	Single photon emission computed tomography
SPIO	Superparamagnetic iron oxide
T_1	Longitudinal relaxation time
T_2	Transverse relaxation time

References

1. Schwarz, S.C.; Schwarz, J. Translation of stem cell therapy for neurological diseases. *Transl. Res.* **2010**, *156*, 155–160. [CrossRef] [PubMed]
2. Mimeault, M.; Batra, S.K. Concise review: Recent avances on the significance of stem cells in tissue regeneration and cancer therapies. *Stem Cells* **2006**, *24*, 2319–2345. [CrossRef]
3. Mimeault, M.; Hauke, R.; Batra, S.K. Stem, Cells: A revolution in therapeutics—Recent advances in stem cell biology and their therapeutic applications in regenerative medicine and cancer therapies. *Clin. Pharmacol. Ther.* **2007**, *82*, 252–264. [CrossRef] [PubMed]
4. NIH Cell Therapies: Completed. Available online: http://www.webcitation.org/6nRZoxwb4 (accessed on 16 January 2017).
5. NIH Cell Therapies: Open. Available online: http://www.webcitation.org/6nRZkihz4 (accessed on 16 January 2017).
6. NIH Cell Therapies in Oncology: Completed. Available online: http://www.webcitation.org/6nRainDln (accessed on 16 January 2017).
7. NIH Cell Therapies in Oncology: Open. Available online: http://www.webcitation.org/6nRb1iPab (accessed on 16 January 2017).
8. Hedlund, E.; Perlmann, T. Neuronal cell replacement in Parkinson's disease. *J. Int. Med.* **2009**, *266*, 358–371. [CrossRef] [PubMed]
9. Baraniak, P.R.; McDevitt, T.C. Stem cell paracrine actions and tissue regeneration. *Regen. Med.* **2010**, *5*, 121–143. [CrossRef] [PubMed]
10. Dittmer, J.; Leyh, B. Paracrine effects of stem cells in wound healing and cancer progression. *Int. J. Oncol.* **2014**, *44*, 1789–1798. [CrossRef] [PubMed]
11. Grealish, S.; Drouin-Ouellet, J.; Parmar, M. Brain repair and reprogramming: The route to clinical translation. *J. Int. Med.* **2016**, *280*, 265–275. [CrossRef] [PubMed]
12. Kim, S.U.; Lee, H.J.; Kim, Y.B. Neural stem cell-based treatment for neurodegenerative diseases. *Neuropathology* **2013**, *33*, 491–504. [CrossRef] [PubMed]
13. Kumar, A.; Narayanan, K.; Chaudhary, R. K.; Mishra, S.; Kumar, S.; Vinoth, K.J.; Padmanabhan, P.; Gulyás, B. Current perspective of stem cell therapy in neurodegenerative and metabolic diseases. *Mol. Neurobiol.* **2016**. [CrossRef] [PubMed]
14. Lescaudron, L.; Naveilhan, P.; Neveu, I. The use of stem cells in regenerative medicine for Parkinson's and Huntington's diseases. *Curr. Med. Chem.* **2012**, *19*, 6018–6035. [CrossRef] [PubMed]
15. Wang, Y.; Chen, S.; Yang, D.; Le, W.D. Stem cell transplantation: A promising therapy for Parkinson's disease. *J. Neuroimmune. Pharmacol.* **2007**, *2*, 243–250. [CrossRef] [PubMed]
16. Francisco, P.M.; Richard, H.W.F. Implications of parkinson's disease pathophysiology for the development of cell replacement strategies and drug discovery in neurodegenerative diseases. *CNS Neurol. Disord. Drug Targets* **2012**, *11*, 907–920.
17. Gibson, S.A.J.; Gao, G.D.; McDonagh, K.; Shen, S. Progress on stem cell research towards the treatment of Parkinson's disease. *Stem Cell Res. Ther.* **2012**, *3*, 11. [CrossRef] [PubMed]
18. Tincer, G.; Mashkaryan, V.; Bhattarai, P.; Kizil, C. Neural stem/progenitor cells in Alzheimer's disease. *Yale J. Biol. Med.* **2016**, *89*, 23–35.
19. Ager, R.R.; Davis, J.L.; Agazaryan, A.; Benavente, F.; Poon, W.W.; LaFerla, F.M.; Blurton-Jones, M. Human neural stem cells improve cognition and promote synaptic growth in two complementary transgenic models of Alzheimer's disease and neuronal loss. *Hippocampus* **2015**, *25*, 813–826. [CrossRef] [PubMed]
20. McGinley, L.M.; Sims, E.; Lunn, J.S.; Kashlan, O.N.; Chen, K.S.; Bruno, E.S.; Pacut, C.M.; Hazel, T.; Johe, K.; Sakowski, S.A.; et al. Human cortical neural stem cells expressing insulin-like growth factor-I: A novel cellular therapy for Alzheimer's disease. *Stem Cells Transl. Med.* **2016**, *5*, 379–391. [CrossRef] [PubMed]
21. Di Ruscio, A.; Patti, F.; Welner, R.S.; Tenen, D.G.; Amabile, G. Multiple sclerosis: Getting personal with induced pluripotent stem cells. *Cell Death Dis.* **2015**, *6*, e1806.
22. Xiao, J.; Yang, R.; Biswas, S.; Qin, X.; Zhang, M.; Deng, W. Mesenchymal, Stem Cells and Induced, Pluripotent Stem, Cells as Therapies for Multiple, Sclerosis. *Int. J. Mol. Sci.* **2015**, *16*, 9283–9302. [CrossRef] [PubMed]
23. Xiang, L.; Chen, Y. Stem cell transplantation for treating spinal cord injury: A literature comparison between studies of stem cells obtained from various sources. *Neural. Regen. Res.* **2012**, *7*, 1256–1263. [PubMed]

24. Boido, M.; Garbossa, D.; Fontanella, M.; Ducati, A.; Vercelli, A. Mesenchymal stem cell transplantation reduces glial cyst and improves functional outcome after spinal cord compression. *World Neurosurg.* **2014**, *81*, 183–190. [CrossRef] [PubMed]
25. Chau, M.J.; Deveau, T.C.; Song, M.; Gu, X.; Chen, D.; Wei, L. iPSC transplantation increases regeneration and functional recovery after ischemic stroke in neonatal rats. *Stem Cells* **2014**, *32*, 3075–3087. [CrossRef] [PubMed]
26. Chang, D.J.; Lee, N.; Park, I.H.; Choi, C.; Jeon, I.; Kwon, J.; Oh, S.H.; Shin, D.A.; Do, J.T.; Lee, D.R.; et al. Therapeutic potential of human induced pluripotent stem cells in experimental stroke. *Cell Transplant.* **2013**, *22*, 1427–1440. [CrossRef] [PubMed]
27. Hao, L.; Zou, Z.; Tian, H.; Zhang, Y.; Zhou, H.; Liu, L. Stem cell-based therapies for ischemic stroke. *BioMed Res. Int.* **2014**. [CrossRef] [PubMed]
28. Peng, W.; Sun, J.; Sheng, C.; Wang, Z.; Wang, Y.; Zhang, C.; Fan, R. Systematic review and meta-analysis of efficacy of mesenchymal stem cells on locomotor recovery in animal models of traumatic brain injury. *Stem Cell Res. Ther.* **2015**, *6*, 1–13. [CrossRef] [PubMed]
29. Gao, X.; Wang, X.; Xiong, W.; Chen, J. In vivo reprogramming reactive glia into iPSCs to produce new neurons in the cortex following traumatic brain injury. *Sci. Rep.* **2016**, *6*, 22490. [CrossRef] [PubMed]
30. Savitz, S.I.; Cox, C.S. Concise review: Cell therapies for stroke and traumatic brain injury: Targeting microglia. *Stem Cells* **2016**, *34*, 537–542. [CrossRef] [PubMed]
31. Ngen, E.J.; Wang, L.; Gandhi, N.; Kato, Y.; Armour, M.; Zhu, W.; Wong, J.; Gabrielson, K.L.; Artemov, D. A preclinical murine model for the early detection of radiation-induced brain injury using magnetic resonance imaging and behavioral tests for learning and memory: With applications for the evaluation of possible stem cell imaging agents and therapies. *J. Neuro Oncol.* **2016**, *128*, 225–233. [CrossRef] [PubMed]
32. Acharya, M.M.; Martirosian, V.; Christie, L.A.; Limoli, C.L. Long-term cognitive effects of human stem cell transplantation in the irradiated brain. *Int. J. Radiat. Biol.* **2014**, *90*, 816–820. [CrossRef] [PubMed]
33. Acharya, M.M.; Rosi, S.; Jopson, T.; Limoli, C.L. Human neural stem cell transplantation provides long-term restoration of neuronal plasticity in the irradiated hippocampus. *Cell Transplant.* **2015**, *24*, 691–702. [CrossRef] [PubMed]
34. Greene-Schloesser, D.; Robbins, M.E. Radiation-induced cognitive impairment-from bench to bedside. *Neuro Oncol.* **2012**, *14*, IV37–IV44. [CrossRef] [PubMed]
35. Piao, J.; Major, T.; Auyeung, G.; Policarpio, E.; Menon, J.; Droms, L.; Gutin, P.; Uryu, K.; Tchieu, J.; Soulet, D.; et al. Human embryonic stem cell-derived oligodendrocyte progenitors remyelinate the brain and rescue behavioral deficits following radiation. *Cell Stem Cell* **2015**, *16*, 198–210. [CrossRef] [PubMed]
36. Hocking, A.M.; Gibran, N.S. Mesenchymal stem cells: Paracrine signaling and differentiation during cutaneous wound repair. *Exp. Cell Res.* **2010**, *316*, 2213–2219. [CrossRef] [PubMed]
37. Wu, Y.; Zhao, R.C.H.; Tredget, E.E. Concise review: Bone marrow-derived stem/progenitor cells in cutaneous repair and regeneration. *Stem Cells* **2010**, *28*, 905–915. [PubMed]
38. Le, T.Y.L.; Chong, J.J.H. Cardiac progenitor cells for heart repair. *Cell Death Discov.* **2016**, *2*, 16052. [PubMed]
39. Lerman, D.A.; Alotti, N.; Ume, K.L.; Péault, B. Cardiac repair and regeneration: The value of cell therapies. *Eur. Cardiol.* **2016**, *11*, 43–48. [CrossRef]
40. Nguyen, P.K.; Rhee, J.; Wu, J.C. Adult stem cell therapy and heart failure, 2000 to 2016: A systematic review. *JAMA Cardiol.* **2016**, *1*, 831–841. [CrossRef] [PubMed]
41. Erbani, J.; Aberdam, D.; Larghero, J.; Vanneaux, V. Pluripotent stem cells and other innovative strategies for the treatment of ocular surface diseases. *Stem Cell Rev.* **2016**, *12*, 171–178. [CrossRef] [PubMed]
42. Gromova, A.; Voronov, D.A.; Yoshida, M.; Thotakura, S.; Meech, R.; Dartt, D.A.; Makarenkova, H.P. Lacrimal gland repair using progenitor cells. *Stem Cells Transl. Med.* **2016**. [CrossRef] [PubMed]
43. Lin, H.; Ouyang, H.; Zhu, J.; Huang, S.; Liu, Z.; Chen, S.; Cao, G.; Li, G.; Signer, R.A.J.; Xu, Y.; et al. Lens regeneration using endogenous stem cells with gain of visual function. *Nature* **2016**, *531*, 323–328. [CrossRef] [PubMed]
44. Omoto, M.; Katikireddy, K.R.; Rezazadeh, A.; Dohlman, T.H.; Chauhan, S.K. Mesenchymal stem cells home to inflamed ocular surface and suppress allosensitization in corneal transplantation M.S.C.s suppress corneal alloimmunity. *Inves. Ophth. Vis. Sci.* **2014**, *55*, 6631–6638. [CrossRef] [PubMed]

45. Liu, W.H.; Ren, L.N.; Wang, T.; Navarro-Alvarez, N.; Tang, L.J. The involving roles of intrahepatic and extrahepatic stem/progenitor cells (SPCs) to liver regeneration. *Int. J. Biol. Sci.* **2016**, *12*, 954–963. [CrossRef] [PubMed]
46. Winkler, S.; Hempel, M.; Brückner, S.; Tautenhahn, H.M.; Kaufmann, R.; Christ, B. Identification of pathways in liver repair potentially targeted by secretory proteins from human mesenchymal stem cells. *Int. J. Mol. Sci.* **2016**, *17*, 1099. [CrossRef] [PubMed]
47. Brady, K.; Dickinson, S.C.; Guillot, P.V.; Polak, J.; Blom, A.W.; Kafienah, W.; Hollander, A.P. Human fetal and adult bone marrow-derived mesenchymal stem cells use different signaling pathways for the initiation of chondrogenesis. *Stem Cells Dev.* **2014**, *23*, 541–554. [CrossRef] [PubMed]
48. Gobbi, A.; Karnatzikos, G.; Sankineani, S.R. One-step surgery with multipotent stem cells for the treatment of large full-thickness chondral defects of the knee. *Am. J. Sport Med.* **2014**, *42*, 648–657. [CrossRef] [PubMed]
49. Ha, C.W.; Park, Y.B.; Chung, J.Y.; Park, Y.G. Cartilage repair using composites of human umbilical cord blood-derived mesenchymal stem cells and hyaluronic acid hydrogel in a minipig model. *Stem Cells Trans. Med.* **2015**, *4*, 1044–1051. [CrossRef] [PubMed]
50. Sekiya, I.; Muneta, T.; Horie, M.; Koga, H. Arthroscopic transplantation of synovial stem cells improves clinical outcomes in knees with cartilage defects. *Clin. Orthop. Relat. Res.* **2015**, *473*, 2316–2326. [CrossRef] [PubMed]
51. Vonk, L.A.; de Windt, T.S.; Kragten, A.H.M.; Beekhuizen, M.; Mastbergen, S.C.; Dhert, W.J.A.; Lafeber, F.P.J.G.; Creemers, L.B.; Saris, D.B.F. Enhanced cell-induced articular cartilage regeneration by chondrons; the influence of joint damage and harvest site. *Osteoarthr. Cartilage* **2014**, *22*, 1910–1917. [CrossRef] [PubMed]
52. Finocchiaro, G.; Pellegatta, S. Immunotherapy with dendritic cells loaded with glioblastoma stem cells: From preclinical to clinical studies. *Cancer Immunol. Immun.* **2016**, *65*, 101–109. [CrossRef] [PubMed]
53. Nava, S.; Lisini, D.; Pogliani, S.; Dossena, M.; Bersano, A.; Pellegatta, S.; Parati, E.; Finocchiaro, G.; Frigerio, S. Safe and reproducible preparation of functional dendritic cells for immunotherapy in glioblastoma patients. *Stem Cells Transl. Med.* **2015**, *4*, 1164–1172. [CrossRef] [PubMed]
54. Batich, K.A.; Swartz, A.M.; Sampson, J.H. Enhancing dendritic cell-based vaccination for highly aggressive glioblastoma. *Expert Opin. Biol. Ther.* **2015**, *15*, 79–94. [CrossRef] [PubMed]
55. Schaller, T.H.; Sampson, J.H. Advances and challenges: Dendritic cell vaccination strategies for glioblastoma. *Expert Rev. Vaccines* **2017**, *16*, 1–10. [CrossRef] [PubMed]
56. Desai, R.; Suryadevara, C.M.; Batich, K.A.; Farber, S.H.; Sanchez-Perez, L.; Sampson, J.H. Emerging immunotherapies for glioblastoma. *Expert Opin. Emerg. Drugs* **2016**, *21*, 133–145. [CrossRef] [PubMed]
57. Xu, Q.; Liu, G.; Yuan, X.; Xu, M.; Wang, H.; Ji, J.; Konda, B.; Black, K.L.; Yu, J.S. Antigen-specific T-cell response from dendritic cell vaccination using cancer stem-like cell-associated antigens. *Stem Cells* **2009**, *27*, 1734–1740. [CrossRef] [PubMed]
58. Ikrame, A.; Elodie, P.; Catherine, S.B.; Audrey, D.; Rodney, M.; Géraldine, L.; Johanne, S.; Eric, T.; François, L.; Philippe, B.; et al. Engineered mesenchymal stem cells as vectors in a suicide gene therapy against preclinical murine models for solid tumors. *J. Control. Release* **2016**, *239*, 82–91.
59. Amara, I.; Touati, W.; Beaune, P.; de Waziers, I. Mesenchymal stem cells as cellular vehicles for prodrug gene therapy against tumors. *Biochimie* **2014**, *105*, 4–11. [CrossRef] [PubMed]
60. Uchibori, R.; Tsukahara, T.; Ohmine, K.; Ozawa, K. Cancer gene therapy using mesenchymal stem cells. *Int. J. Hematol.* **2014**, *99*, 377–382. [CrossRef] [PubMed]
61. Montserrat, E.; Dreger, P. Treatment of chronic lymphocytic leukemia with del (17p)/ TP53 mutation: Allogeneic hematopoietic stem cell transplantation or BCR-signaling inhibitors? *Clin. Lymphoma Myeloma Leuk.* **2016**, *16*, S74–S81. [CrossRef] [PubMed]
62. Testa, U.; Saulle, E.; Castelli, G.; Pelosi, E. Endothelial progenitor cells in hematologic malignancies. *Stem Cell Investig.* **2016**, *3*, 26. [CrossRef] [PubMed]
63. Kircher, M.F.; Gambhir, S.S.; Grimm, J. Noninvasive cell-tracking methods. *Nat. Rev. Clin. Oncol.* **2011**, *8*, 677–688. [CrossRef] [PubMed]
64. Naumova, A.V.; Modo, M.; Moore, A.; Murry, C.E.; Frank, J.A. Clinical imaging in regenerative medicine. *Nat. Biotech.* **2014**, *32*, 804–818. [CrossRef] [PubMed]
65. Liu, W.; Frank, J.A. Detection and quantification of magnetically labeled cells by cellular MRI. *Eur. J. Radiol.* **2009**, *70*, 258–264. [CrossRef] [PubMed]

66. Shapiro, E.M.; Sharer, K.; Skrtic, S.; Koretsky, A.P. In vivo detection of single cells by MRI. *Magn. Reson. Med.* **2006**, *55*, 242–249. [CrossRef] [PubMed]
67. Makela, A.V.; Murrell, D.H.; Parkins, K.M.; Kara, J.; Gaudet, J.M.; Foster, P.J. Cellular, Imaging With, MRI. *Top. Magn. Reson. Imaging* **2016**, *25*, 177–186. [CrossRef] [PubMed]
68. Frank, J.A.; Miller, B.R.; Arbab, A.S.; Zywicke, H.A.; Jordan, E.K.; Lewis, B.K.; Bryant, L.H.; Bulte, J.W.M. Clinically applicable labeling of mammalian and stem cells by combining superparamagnetic iron oxides and transfection agents. *Radiology* **2003**, *228*, 480–487. [CrossRef] [PubMed]
69. Kalish, H.; Arbab, A.S.; Miller, B.R.; Lewis, B.K.; Zywicke, H.A.; Bulte, J.W.M.; Bryant, L.H.; Frank, J.A. Combination of transfection agents and magnetic resonance contrast agents for cellular imaging: Relationship between relaxivities, electrostatic forces, and chemical composition. *Magn. Reson. Med.* **2003**, *50*, 275–282. [CrossRef] [PubMed]
70. Ahrens, E.T.; Flores, R.; Xu, H.; Morel, P.A. In vivo imaging platform for tracking immunotherapeutic cells. *Nat. Biotech.* **2005**, *23*, 983–987. [CrossRef]
71. Qiu, B.; Xie, D.; Walczak, P.; Li, X.; Ruiz-Cabello, J.; Minoshima, S.; Bulte, J.W.M.; Yang, X. Magnetosonoporation: Instant magnetic labeling of stem cells. *Magn. Reson. Med.* **2010**, *63*, 1437–1441. [CrossRef] [PubMed]
72. Walczak, P.; Kedziorek, D.A.; Gilad, A.A.; Lin, S.; Bulte, J.W.M. Instant, MR labeling of stem cells using magnetoelectroporation. *Magn. Reson. Med.* **2005**, *54*, 769–774. [CrossRef] [PubMed]
73. Walczak, P.; Ruiz-Cabello, J.; Kedziorek, D.A.; Gilad, A.A.; Lin, S.; Barnett, B.; Qin, L.; Levitsky, H.; Bulte, J.W.M. Magnetoelectroporation: Improved labeling of neural stem cells and leukocytes for cellular magnetic resonance imaging using a single FDA-approved agent. *Nanomedicine* **2006**, *2*, 89–94. [CrossRef] [PubMed]
74. Granot, D.; Scheinost, D.; Markakis, E.A.; Papademetris, X.; Shapiro, E.M. Serial monitoring of endogenous neuroblast migration by cellular MRI. *Neuroimage* **2011**, *57*, 817–824. [CrossRef] [PubMed]
75. Jefferson, A.; Wijesurendra, R.S.; McAteer, M.A.; Choudhury, R.P. Development and application of endothelium-targeted microparticles for molecular magnetic resonance imaging. *Wiley Interdiscip. Rev. Nanomed. Nanobiotechnol.* **2012**, *4*, 247–256. [CrossRef] [PubMed]
76. McAteer, M.A.; Schneider, J.E.; Ali, Z.A.; Warrick, N.; Bursill, C.A.; von zur Muhlen, C.; Greaves, D.R.; Neubauer, S.; Channon, K.M.; Choudhury, R.P. Magnetic resonance imaging of endothelial adhesion molecules in mouse atherosclerosis using dual-targeted microparticles of iron oxide. *Arterioscler. Thromb. Vasc. Biol.* **2008**, *28*, 77–83. [CrossRef] [PubMed]
77. McAteer, M.A.; Mankia, K.; Ruparelia, N.; Jefferson, A.; Nugent, H.B.; Stork, L.A.; Channon, K.M.; Schneider, J.E.; Choudhury, R.P. A leukocyte-mimetic magnetic resonance imaging contrast agent homes rapidly to activated endothelium and tracks with atherosclerotic lesion macrophage content. *Arterioscler. Thromb. Vasc. Biol.* **2012**, *32*, 1427–1435. [CrossRef] [PubMed]
78. Tu, C.; Ng, T.S.C.; Sohi, H.; Palko, H.; House, A.; Jacobs, R.E.; Louie, A.Y. Receptor-targeted iron oxide nanoparticles for molecular MR imaging of inflamed atherosclerotic plaques. *Biomaterials* **2011**, *32*, 7209–7216. [CrossRef] [PubMed]
79. Chen, C.L.; Siow, T.Y.; Chou, C.H.; Lin, C.H.; Lin, M.H.; Chen, Y.C.; Hsieh, W.Y.; Wang, S.J.; Chang, C. Targeted superparamagnetic iron oxide nanoparticles for in vivo magnetic resonance imaging of T-cells in rheumatoid arthritis. *Mol. Imaging Biol.* **2016**. [CrossRef] [PubMed]
80. Liu, L.; Ye, Q.; Wu, Y.; Hsieh, W.Y.; Chen, C.L.; Shen, H.H.; Wang, S.J.; Zhang, H.; Hitchens, T.K.; Ho, C. Tracking, T-cells in vivo with a new nano-sized MRI contrast agent. *Nanomedicine* **2012**, *8*, 1345–1354. [CrossRef] [PubMed]
81. Zhang, F.; Duan, X.; Lu, L.; Zhang, X.; Zhong, X.; Mao, J.; Chen, M.; Shen, J. In vivo targeted MR imaging of endogenous neural stem cells in ischemic stroke. *Molecules* **2016**, *21*, 1143. [CrossRef] [PubMed]
82. Khurana, A.; Chapelin, F.; Beck, G.; Lenkov, O.D.; Donig, J.; Nejadnik, H.; Messing, S.; Derugin, N.; Chan, R.C.F.; Gaur, A.; et al. Iron administration before stem cell harvest enables MR imaging tracking after transplantation. *Radiology* **2013**, *269*, 186–197. [CrossRef] [PubMed]
83. Bulte, J.W.M. Science to practice: Can stem cells be labeled inside the body instead of outside? *Radiology* **2013**, *269*, 1–3. [CrossRef] [PubMed]

84. Winter, E.M.; Hogers, B.; van der Graaf, L.M.; Gittenberger-de Groot, A.C.; Poelmann, R.E.; van der Weerd, L. Cell tracking using iron oxide fails to distinguish dead from living transplanted cells in the infarcted heart. *Magn. Reson. Med.* **2010**, *63*, 817–821. [CrossRef] [PubMed]
85. Cianciaruso, C.; Pagani, A.; Martelli, C.; Bacigaluppi, M.; Leonardo Squadrito, M.; lo Dico, A.; de Palma, M.; Furlan, R.; Lucignani, G.; Falini, A.; et al. Cellular magnetic resonance with iron oxide nanoparticles: Long-term persistence of SPIO signal in the CNS after transplanted cell death. *Nanomedicine* **2014**, *9*, 1457–1474. [CrossRef] [PubMed]
86. Naumova, A.V.; Balu, N.; Yarnykh, V.L.; Reinecke, H.; Murry, C.E.; Yuan, C. Magnetic resonance imaging tracking of graft survival in the infarcted heart: Iron oxide particles versus ferritin overexpression approach. *J. Cardiovasc. Pharmacol. Ther.* **2014**, *19*, 358–367. [CrossRef] [PubMed]
87. Terrovitis, J.; Stuber, M.; Youssef, A.; Preece, S.; Leppo, M.; Kizana, E.; Schär, M.; Gerstenblith, G.; Weiss, R.G.; Marbán, E.; et al. Magnetic resonance imaging overestimates ferumoxide-labeled stem cell survival after transplantation in the heart. *Circulation* **2008**, *117*, 1555–1562. [CrossRef] [PubMed]
88. Ngen, E.J.; Wang, L.; Kato, Y.; Krishnamachary, B.; Zhu, W.; Gandhi, N.; Smith, B.; Armour, M.; Wong, J.; Gabrielson, K.; et al. Imaging transplanted stem cells in real time using an MRI dual-contrast method. *Sci. Rep.* **2015**, *5*, 13628. [CrossRef] [PubMed]
89. Henning, T.D.; Wendland, M.F.; Golovko, D.; Sutton, E.J.; Sennino, B.; Malek, F.; Bauer, J.S.; McDonald, D.M.; Daldrup-Link, H. Relaxation effects of ferucarbotran-labeled mesenchymal stem cells at 1.5 T and 3 T: Discrimination of viable from lysed cells. *Magn. Reson. Med.* **2009**, *62*, 325–332. [CrossRef] [PubMed]
90. Guenoun, J.; Ruggiero, A.; Doeswijk, G.; Janssens, R.C.; Koning, G.A.; Kotek, G.; Krestin, G.P.; Bernsen, M.R. In vivo quantitative assessment of cell viability of gadolinium or iron-labeled cells using MRI and bioluminescence imaging. *Contrast Media Mol.* **2013**, *8*, 165–174. [CrossRef] [PubMed]
91. Tachibana, Y.; Enmi, J.; Agudelo, C.A.; Iida, H.; Yamaoka, T. Long-Term/Bioinert, Labeling of Rat, Mesenchymal Stem, Cells with PVA-Gd, Conjugates and MRI Monitoring of the Labeled, Cell Survival after Intramuscular, Transplantation. *Bioconjug. Chem.* **2014**, *25*, 1243–1251. [CrossRef] [PubMed]
92. Ribot, E.J.; Foster, P.J. In vivo MRI discrimination between live and lysed iron-labelled cells using balanced steady state free precession. *Eur. Radiol.* **2012**, *22*, 2027–2034. [CrossRef] [PubMed]
93. Chan, K.W.Y.; Liu, G.; Song, X.; Kim, H.; Yu, T.; Arifin, D.R.; Gilad, A.A.; Hanes, J.; Walczak, P.; van Zijl, P.C.M.; et al. MRI-detectable pH nanosensors incorporated into hydrogels for in vivo sensing of transplanted-cell viability. *Nat. Mater.* **2013**, *12*, 268–275. [CrossRef] [PubMed]
94. Ngen, E.J.; Bar-Shir, A.; Jablonska, A.; Liu, G.; Song, X.; Ansari, R.; Bulte, J.W.M.; Janowski, M.; Pearl, M.; Walczak, P.; et al. Imaging the DNA alkylator melphalan by CEST MRI An advanced approach to theranostics. *Mol. Pharm.* **2016**, *13*, 3043–3053. [CrossRef] [PubMed]
95. Berman, S.C.; Galpoththawela, C.; Gilad, A.A.; Bulte, J.W.M.; Walczak, P. Long-term MR cell tracking of neural stem cells grafted in immunocompetent versus immunodeficient mice reveals distinct differences in contrast between live and dead cells. *Magn. Reson. Med.* **2011**, *65*, 564–574. [CrossRef] [PubMed]
96. Gilad, A.A.; Winnard, P.T.; van Zijl, P.C.M.; Bulte, J.W.M. Developing, MR reporter genes: Promises and pitfalls. *N.M.R. Biomed.* **2007**, *20*, 275–290. [CrossRef] [PubMed]
97. Gilad, A.A.; Ziv, K.; McMahon, M.T.; van Zijl, P.C.M.; Neeman, M.; Bulte, J.W.M. MRI reporter genes. *J. Nucl. Med.* **2008**, *49*, 1905–1908. [CrossRef] [PubMed]
98. Cohen, B.; Ziv, K.; Plaks, V.; Israely, T.; Kalchenko, V.; Harmelin, A.; Benjamin, L.E.; Neeman, M. MRI detection of transcriptional regulation of gene expression in transgenic mice. *Nat. Med.* **2007**, *13*, 498–503. [CrossRef] [PubMed]
99. Genove, G.; DeMarco, U.; Xu, H.; Goins, W.F.; Ahrens, E.T. A new transgene reporter for in vivo magnetic resonance imaging. *Nat. Med.* **2005**, *11*, 450–454. [CrossRef] [PubMed]
100. Liu, J.; Cheng, E.C.H.; Long, R.C.; Yang, S.H.; Wang, L.; Cheng, P.H.; Yang, J.; Wu, D.; Mao, H.; Chan, A.W.S. Noninvasive monitoring of embryonic stem cells in vivo with MRI transgene reporter. *Tissue Eng. Part C Methods* **2009**, *15*, 739–747. [CrossRef] [PubMed]
101. Louie, A.Y.; Huber, M.M.; Ahrens, E.T.; Rothbacher, U.; Moats, R.; Jacobs, R.E.; Fraser, S.E.; Meade, T.J. In vivo visualization of gene expression using magnetic resonance imaging. *Nat. Biotechnol.* **2000**, *18*, 321–325. [PubMed]

102. Bar-Shir, A.; Liang, Y.; Chan, K.W.Y.; Gilad, A.A.; Bulte, J.W.M. Supercharged green fluorescent proteins as bimodal reporter genes for CEST MRI and optical imaging. *Chem. Commun.* **2015**, *51*, 4869–4871. [CrossRef] [PubMed]
103. Bar-Shir, A.; Liu, G.; Chan, K.W.; Oskolkov, N.; Song, X.; Yadav, N.N.; Walczak, P.; McMahon, M.T.; van Zijl, P.C.; Bulte, J.W.; et al. Human protamine-1 as an MRI reporter gene based on chemical exchange. *ACS Chem. Biol.* **2014**, *9*, 134–138. [CrossRef] [PubMed]
104. Gilad, A.A.; McMahon, M.T.; Walczak, P.; Winnard, P.T.; Raman, V.; van Laarhoven, H.W.M.; Skoglund, C.M.; Bulte, J.W.M.; van Zijl, P.C.M. Artificial reporter gene providing MRI contrast based on proton exchange. *Nat. Biotechnol.* **2007**, *25*, 217–219. [CrossRef] [PubMed]
105. Airan, R.D.; Bar-Shir, A.; Liu, G.; Pelled, G.; McMahon, M.T.; van Zijl, P.C.M.; Bulte, J.W.M.; Gilad, A.A. MRI biosensor for protein kinase A encoded by a single synthetic gene. *Magn. Reson. Med.* **2012**, *68*, 1919–1923. [CrossRef] [PubMed]
106. Bar-Shir, A.; Liu, G.; Liang, Y.; Yadav, N.N.; McMahon, M.T.; Walczak, P.; Nimmagadda, S.; Pomper, M.G.; Tallman, K.A.; Greenberg, M.M.; et al. Transforming thymidine into a magnetic resonance imaging probe for monitoring gene expression. *J. Am. Chem. Soc.* **2013**, *135*, 1617–1624. [CrossRef] [PubMed]
107. Liu, G.; Liang, Y.; Bar-Shir, A.; Chan, K.W.Y.; Galpoththawela, C.S.; Bernard, S.M.; Tse, T.; Yadav, N.N.; Walczak, P.; McMahon, M.T.; et al. Monitoring enzyme activity using a diamagnetic chemical exchange saturation transfer magnetic resonance imaging contrast agent. *J. Am. Chem. Soc.* **2011**, *133*, 16326–16329. [CrossRef] [PubMed]
108. Arifin, D.R.; Kedziorek, D.A.; Fu, Y.; Chan, K.W.Y.; McMahon, M.T.; Weiss, C.R.; Kraitchman, D.L.; Bulte, J.W.M. Microencapsulated cell tracking. *NMR Biomed.* **2013**, *26*, 850–859. [CrossRef] [PubMed]
109. Paredes-Juarez, G.A.; Barnett, B.P.; Bulte, J.W.M. Noninvasive tracking of alginate-microencapsulated cells. In *Cell Microencapsulation: Methods and Protocols*; Opara, E.C., Ed.; Springer: New York, NY, USA, 2017; pp. 143–155.
110. Barnett, B.P.; Arepally, A.; Stuber, M.; Arifin, D.R.; Kraitchman, D.L.; Bulte, J.W.M. Synthesis of magnetic resonance–, X-ray– and ultrasound-visible alginate microcapsules for immunoisolation and noninvasive imaging of cellular therapeutics. *Nat. Protoc.* **2011**, *6*, 1142–1151. [CrossRef] [PubMed]
111. Arifin, D.R.; Valdeig, S.; Anders, R.A.; Bulte, J.W.M.; Weiss, C.R. Magnetoencapsulated human islets xenotransplanted into swine: A comparison of different transplantation sites. *Xenotransplantation* **2016**, *23*, 211–221. [CrossRef] [PubMed]
112. Fu, Y.; Azene, N.; Ehtiati, T.; Flammang, A.; Gilson, W.D.; Gabrielson, K.; Weiss, C.R.; Bulte, J.W.M.; Solaiyappan, M.; Johnston, P.V.; et al. Fused, X-ray and MR Imaging guidance of intrapericardial delivery of microencapsulated human mesenchymal stem cells in immunocompetent swine. *Radiology* **2014**, *272*, 427–437. [CrossRef] [PubMed]
113. Bulte, J.W.M. In vivo MRI cell tracking: Clinical studies. *Am. J. Roentgenol.* **2009**, *193*, 314–325. [CrossRef] [PubMed]
114. Evgenov, N.V.; Medarova, Z.; Dai, G.; Bonner-Weir, S.; Moore, A. In vivo imaging of islet transplantation. *Nat. Med.* **2006**, *12*, 144–148. [CrossRef] [PubMed]
115. Kraitchman, D.L.; Kedziorek, D.A.; Bulte, J.W.M. MR Imaging of transplanted stem cells in myocardial infarction molecular imaging. In *Molecular Imaging*; Shah, K., Ed.; Humana Press: New York, NY, USA, 2011; pp. 141–152.
116. Mao, X.; Xu, J.; Cui, H. Functional nanoparticles for magnetic resonance imaging. *Wiley Interdiscip. Rev. Nanomed. Nanobiotechnol.* **2016**. [CrossRef] [PubMed]
117. De León-Rodríguez, L.M.; Martins, A.F.; Pinho, M.C.; Rofsky, N.M.; Sherry, A.D. Basic, MR relaxation mechanisms and contrast agent design. *J. Magn. Reson. Imaging* **2015**, *42*, 545–565. [CrossRef] [PubMed]
118. Kraitchman, D.L.; Caravan, P. Magnetic resonance labeling of stem cells: Is positive tracking a plus or a minus? *JACC Cardiovasc. Imaging* **2009**, *2*, 1123–1125. [CrossRef] [PubMed]
119. Cromer Berman, S.M.; Walczak, P.; Bulte, J.W.M. Tracking stem cells using magnetic nanoparticles. *Wiley Interdiscip. Rev. Nanomed. Nanobiotechnol.* **2011**, *3*, 343–355.
120. Qi, Y.; Feng, G.; Huang, Z.; Yan, W. The application of super paramagnetic iron oxide-labeled mesenchymal stem cells in cell-based therapy. *Mol. Biol. Rep.* **2013**, *40*, 2733–2740. [CrossRef] [PubMed]

121. Srivastava, A.K.; Kadayakkara, D.K.; Bar-Shir, A.; Gilad, A.A.; McMahon, M.T.; Bulte, J.W.M. Advances in using MRI probes and sensors for in vivo cell tracking as applied to regenerative medicine. *Dis. Model. Mech.* **2015**, *8*, 323–336. [CrossRef] [PubMed]
122. Reimer, P.; Balzer, T. Ferucarbotran (Resovist): A new clinically approved RES-specific contrast agent for contrast-enhanced MRI of the liver: Properties, clinical development, and applications. *Eur. Radiol.* **2003**, *13*, 1266–1276. [PubMed]
123. Coyne, D.W. Ferumoxytol for treatment of iron deficiency anemia in patients with chronic kidney disease. *Expert Opin. Pharmacother.* **2009**, *10*, 2563–2568. [CrossRef] [PubMed]
124. Castaneda, R.T.; Khurana, A.; Khan, R.; Daldrup-Link, H.E. Labeling stem cells with ferumoxytol, an FDA-approved iron oxide nanoparticle. *J. Vis. Exp.* **2011**, 3482. [CrossRef] [PubMed]
125. Granot, D.; Nkansah, M.K.; Bennewitz, M.F.; Tang, K.S.; Markakis, E.A.; Shapiro, E.M. Clinically viable magnetic poly(lactide-co-glycolide) (PLGA) particles for MRI-based cell tracking. *Magn. Reson. Med.* **2014**, *71*, 1238–1250. [CrossRef] [PubMed]
126. Shapiro, E.M. Biodegradable, polymer encapsulated, metal oxide particles for MRI-based cell tracking. *Magn. Reson. Med.* **2015**, *73*, 376–389. [CrossRef] [PubMed]
127. Lü, J.M.; Wang, X.; Marin-Muller, C.; Wang, H.; Lin, P.H.; Yao, Q.; Chen, C. Current advances in research and clinical applications of PLGA-based nanotechnology. *Exp. Rev. Mol. Diagn.* **2009**, *9*, 325–341. [CrossRef] [PubMed]
128. Nkansah, M.K.; Thakral, D.; Shapiro, E.M. Magnetic poly(lactide-co-glycolide) and cellulose particles for MRI-based cell tracking. *Magn. Reson. Med.* **2011**, *65*, 1776–1785. [CrossRef] [PubMed]
129. Louie, A. MRI biosensors: A short primer. *J. Magn. Reson. Imaging* **2013**, *38*, 530–539. [CrossRef] [PubMed]
130. Shapiro, E.M.; Skrtic, S.; Koretsky, A.P. Sizing it up: Cellular, MRI using micron-sized iron oxide particles. *Magn. Reson. Med.* **2005**, *53*, 329–338. [CrossRef] [PubMed]
131. Leder, A.; Raschzok, N.; Schmidt, C.; Arabacioglu, D.; Butter, A.; Kolano, S.; de Sousa Lisboa, L.S.; Werner, W.; Polenz, D.; Reutzel-Selke, A.; et al. Micron-sized iron oxide-containing particles for microRNA-targeted manipulation and MRI-based tracking of transplanted cells. *Biomaterials* **2015**, *51*, 129–137. [CrossRef] [PubMed]
132. Iordanova, B.; Robison, C.; Goins, W.; Ahrens, E. Single chain ferritin chimera as an improved MRI gene reporter. *Prilozi* **2010**, *31*, 151–155. [PubMed]
133. Cohen, B.; Ziv, K.; Plaks, V.; Harmelin, A.; Neeman, M. Ferritin nanoparticles as magnetic resonance reporter gene. *Wiley Interdiscip. Rev. Nanomed. Nanobiotechnol.* **2009**, *1*, 181–188. [CrossRef] [PubMed]
134. Matsumoto, Y.; Chen, R.; Anikeeva, P.; Jasanoff, A. Engineering intracellular biomineralization and biosensing by a magnetic protein. *Nat. Commun.* **2015**, *6*, 8721. [CrossRef] [PubMed]
135. Kim, H.S.; Woo, J.; Choi, Y.; Hwang, E.H.; Choi, S.K.; Cho, K.W.; Moon, W.K. Noninvasive, MRI and multilineage differentiation capability of ferritin-transduced human mesenchymal stem cells. *NMR Biomed.* **2015**, *28*, 168–179. [CrossRef] [PubMed]
136. Noad, J.; Gonzalez-Lara, L.E.; Broughton, H.C.; McFadden, C.; Chen, Y.; Hess, D.A.; Foster, P.J. MRI tracking of transplanted iron-labeled mesenchymal stromal cells in an immune-compromised mouse model of critical limb ischemia. *NMR Biomed.* **2013**, *26*, 458–467. [CrossRef] [PubMed]
137. Nedopil, A.; Klenk, C.; Kim, C.; Liu, S.; Wendland, M.; Golovko, D.; Schuster, T.; Sennino, B.; McDonald, D.M.; Daldrup-Link, H.E. MR signal characteristics of viable and apoptotic human mesenchymal stem cells in MASI for treatment of osteoarthritis. *Invest. Radiol.* **2010**, *45*, 634–640. [CrossRef] [PubMed]
138. Van Buul, G.M.; Kotek, G.; Wielopolski, P.A.; Farrell, E.; Bos, P.K.; Weinans, H.; Grohnert, A.U.; Jahr, H.; Verhaar, J.A.N.; Krestin, G.P.; et al. Clinically translatable cell tracking and quantification by MRI in cartilage repair using superparamagnetic iron oxides. *PLoS ONE* **2011**, *6*, e17001. [CrossRef] [PubMed]
139. Hingorani, D.V.; Bernstein, A.S.; Pagel, M.D. A review of responsive MRI contrast agents: 2005–2014. *Contrast Media Mol. Imaging* **2015**, *10*, 245–265. [CrossRef] [PubMed]
140. Tu, C.; Osborne, E.A.; Louie, A.Y. Activatable, T_1 and T_2 magnetic resonance imaging contrast agents. *Ann. Biomed. Eng.* **2011**, *39*, 1335–1348. [CrossRef] [PubMed]

141. Kato, Y.; Artemov, D. Monitoring of release of cargo from nanocarriers by MRI/MR spectroscopy (MRS): Significance of T_2/T_2^* effect of iron particles. *Magn. Reson. Med.* **2009**, *61*, 1059–1065. [CrossRef] [PubMed]
142. Onuki, Y.; Jacobs, I.; Artemov, D.; Kato, Y. Noninvasive visualization of in vivo release and intratumoral distribution of surrogate MR contrast agent using the dual MR contrast technique. *Biomaterials* **2010**, *31*, 7132–7138. [CrossRef] [PubMed]
143. Kim, T.; Momin, E.; Choi, J.; Yuan, K.; Zaidi, H.; Kim, J.; Park, M.; Lee, N.; McMahon, M.T.; Quinones-Hinojosa, A.; et al. Mesoporous silica-coated hollow manganese oxide nanoparticles as positive T_1 contrast agents for labeling and MRI tracking of adipose-derived mesenchymal stem cells. *J. Am. Chem. Soc.* **2011**, *133*, 2955–2961. [CrossRef] [PubMed]
144. Létourneau, M.; Tremblay, M.; Faucher, L.; Rojas, D.; Chevallier, P.; Gossuin, Y.; Lagueux, J.; Fortin, M.-A. MnO-labeled cells: Positive contrast enhancement in MRI. *J. Phys. Chem. B* **2012**, *116*, 13228–13238. [CrossRef] [PubMed]
145. Guillet-Nicolas, R.; Laprise-Pelletier, M.; Nair, M.M.; Chevallier, P.; Lagueux, J.; Gossuin, Y.; Laurent, S.; Kleitz, F.; Fortin, M.A. Manganese-impregnated mesoporous silica nanoparticles for signal enhancement in MRI cell labelling studies. *Nanoscale* **2013**, *5*, 11499–11511. [CrossRef] [PubMed]
146. Shen, Y.; Shao, Y.; He, H.; Tan, Y.; Tian, X.; Xie, F.; Li, L. Gadolinium^{3+}-doped mesoporous silica nanoparticles as a potential magnetic resonance tracer for monitoring the migration of stem cells in vivo. *Int. J. Nanomed.* **2013**, *8*, 119–127.
147. Hsiao, J.K.; Tsai, C.P.; Chung, T.H.; Hung, Y.; Yao, M.; Liu, H.M.; Mou, C.Y.; Yang, C.S.; Chen, Y.C.; Huang, D.M. Mesoporous silica nanoparticles as a delivery system of gadolinium for effective human stem cell tracking. *Small* **2008**, *4*, 1445–1452. [CrossRef] [PubMed]
148. Guenoun, J.; Koning, G.A.; Doeswijk, G.; Bosman, L.; Wielopolski, P.A.; Krestin, G.P.; Bernsen, M.R. Cationic, Gd-DTPA liposomes for highly efficient labeling of mesenchymal stem cells and cell tracking with MRI. *Cell Transplant.* **2012**, *21*, 191–205. [CrossRef]
149. Hedlund, A.; Ahrén, M.; Gustafsson, H.; Abrikossova, N.; Warntjes, M.; Jönsson, J.I.; Uvdal, K.; Engström, M. Gd_2O_3 nanoparticles in hematopoietic cells for MRI contrast enhancement. *Int. J. Nanomed.* **2011**, *6*, 3233–3240.
150. Gianolio, E.; Arena, F.; Strijkers, G.J.; Nicolay, K.; Högset, A.; Aime, S. Photochemical activation of endosomal escape of MRI-Gd-agents in tumor cells. *Magn. Reson. Med.* **2011**, *65*, 212–219. [CrossRef]
151. Terreno, E.; Geninatti Crich, S.; Belfiore, S.; Biancone, L.; Cabella, C.; Esposito, G.; Manazza, A.D.; Aime, S. Effect of the intracellular localization of a Gd-based imaging probe on the relaxation enhancement of water protons. *Magn. Reson. Med.* **2006**, *55*, 491–497. [CrossRef] [PubMed]
152. Nejadnik, H.; Ye, D.; Lenkov, O.D.; Donig, J.S.; Martin, J.E.; Castillo, R.; Derugin, N.; Sennino, B.; Rao, J.; Daldrup-Link, H. Magnetic resonance imaging of stem cell apoptosis in arthritic joints with a caspase activatable contrast agent. *ACS Nano* **2015**, *9*, 1150–1160. [CrossRef] [PubMed]
153. Regueiro-Figueroa, M.; Gündüz, S.; Patinec, V.; Logothetis, N.K.; Esteban-Gómez, D.; Tripier, R.; Angelovski, G.; Platas-Iglesias, C. Gd^{3+}-Based magnetic resonance imaging contrast agent responsive to Zn^{2+}. *Inorg. Chem.* **2015**, *54*, 10342–10350. [CrossRef] [PubMed]
154. Tu, C.; Louie, A.Y. Strategies for the development of Gd-based "*q*"-activatable MRI contrast agents. *NMR Biomed.* **2013**, *26*, 781–787. [CrossRef] [PubMed]
155. Chang, Y.T.; Cheng, C.M.; Su, Y.Z.; Lee, W.T.; Hsu, J.S.; Liu, G.C.; Cheng, T.L.; Wang, Y.M. Synthesis and characterization of a new bioactivated paramagnetic gadolinium(III) complex [Gd(DOTA-FPG)(H2O)] for tracing gene expression. *Bioconjug. Chem.* **2007**, *18*, 1716–1727. [CrossRef] [PubMed]
156. Duimstra, J.A.; Femia, F.J.; Meade, T.J. A gadolinium chelate for detection of β-glucuronidase: A self-Immolative approach. *J. Am. Chem. Soc.* **2005**, *127*, 12847–12855. [CrossRef] [PubMed]
157. Fujisaki, K.; Ono-Fujisaki, A.; Kura-Nakamura, N.; Komune, N.; Hirakawa, N.; Tsuruya, N.; Komune, S.; Lida, M. Rapid deterioration of renal insufficiency after magnetic resonance imaging with gadolinium-based contrast agent. *Clin. Nephrol.* **2011**, *75*, 251–254. [CrossRef] [PubMed]
158. Buhaescu, I.; Izzedine, H. Gadolinium-induced nephrotoxicity. *Int. J. Clin. Pract.* **2008**, *62*, 1113–1118. [CrossRef] [PubMed]

159. Bar-Shir, A.; Bulte, J.W.M.; Gilad, A.A. Molecular engineering of nonmetallic biosensors for CEST MRI. *ACS Chem. Biol.* **2015**, *10*, 1160–1170. [CrossRef] [PubMed]
160. Sherry, A.D.; Woods, M. Chemical exchange saturation transfer contrast agents for magnetic resonance imaging. *Ann. Rev. Biomed. Eng.* **2008**, *10*, 391–411. [CrossRef] [PubMed]
161. Hancu, I.; Dixon, W.T.; Woods, M.; Vinogradov, E.; Sherry, A.D.; Lenkinski, R.E. CEST and PARACEST MR contrast agents. *Acta Radiol.* **2010**, *51*, 910–923. [CrossRef] [PubMed]
162. Nicholls, F.J.; Ling, W.; Ferrauto, G.; Aime, S.; Modo, M. Simultaneous, MR imaging for tissue engineering in a rat model of stroke. *Sci. Rep.* **2015**, *5*, 14597. [CrossRef] [PubMed]
163. Wang, Y.; Roose, B.W.; Palovcak, E.J.; Carnevale, V.; Dmochowski, I.J. A genetically encoded β-lactamase reporter for ultrasensitive 129Xe, NMR in mammalian cells. *Angew. Chem.* **2016**, *55*, 8984–8987. [CrossRef] [PubMed]
164. Shapiro, M.G.; Ramirez, R.M.; Sperling, L.J.; Sun, G.; Sun, J.; Pines, A.; Schaffer, D.V.; Bajaj, V.S. Genetically encoded reporters for hyperpolarized xenon magnetic resonance imaging. *Nat. Chem.* **2014**, *6*, 629–634. [CrossRef] [PubMed]
165. Bai, Y.; Hill, P.A.; Dmochowski, I.J. Utilizing a water-soluble cryptophane with fast xenon exchange rates for picomolar sensitivity NMR measurements. *Anal. Chem.* **2012**, *84*, 9935–9941. [CrossRef] [PubMed]
166. Stevens, T.K.; Palaniappan, K.K.; Ramirez, R.M.; Francis, M.B.; Wemmer, D.E.; Pines, A. HyperCEST detection of a 129Xe-based contrast agent composed of cryptophane—A molecular cages on a bacteriophage scaffold. *Magn. Reson. Med.* **2013**, *69*, 1245–1252. [CrossRef] [PubMed]
167. Taratula, O.; Dmochowski, I.J. Functionalized 129Xe contrast agents for magnetic resonance imaging. *Curr. Opin. Chem. Biol.* **2010**, *14*, 97–104. [CrossRef] [PubMed]
168. Stevens, T.K.; Ramirez, R.M.; Pines, A. Nanoemulsion contrast agents with sub-picomolar sensitivity for xenon NMR. *J. Am. Chem. Soc.* **2013**, *135*, 9576–9579. [CrossRef] [PubMed]
169. Ahrens, E.T.; Bulte, J.W.M. Tracking immune cells in vivo using magnetic resonance imaging. *Nat. Rev. Immunol.* **2013**, *13*, 755–763. [CrossRef] [PubMed]
170. Srinivas, M.; Boehm-Sturm, P.; Figdor, C.G.; de Vries, I.J.; Hoehn, M. Labeling cells for in vivo tracking using ^{19}F MRI. *Biomaterials* **2012**, *33*, 8830–8840. [CrossRef] [PubMed]
171. Srinivas, M.; Heerschap, A.; Ahrens, E.T.; Figdor, C.G.; de Vries, I.J.M. ^{19}F MRI for quantitative in vivo cell tracking. *Trends Biotechnol.* **2010**, *28*, 363–370. [CrossRef] [PubMed]
172. Ahrens, E.T.; Helfer, B.M.; O'Hanlon, C.F.; Schirda, C. Clinical cell therapy imaging using a perfluorocarbon tracer and fluorine-19 MRI. *Magn. Reson. Med.* **2014**, *72*, 1696–1701. [CrossRef] [PubMed]
173. Kislukhin, A.A.; Xu, H.; Adams, S.R.; Narsinh, K.H.; Tsien, R.Y.; Ahrens, E.T. Paramagnetic fluorinated nanoemulsions for sensitive cellular fluorine-19 magnetic resonance imaging. *Nat. Mater.* **2016**, *15*, 662–668. [CrossRef] [PubMed]
174. Hockett, F.D.; Wallace, K.D.; Schmieder, A.H.; Caruthers, S.D.; Pham, C.T.N.; Wickline, S.A.; Lanza, G.M. Simultaneous, dual frequency ^{1}H and ^{19}F open, coil imaging of arthritic, rabbit knee at 3 T. *IEEE Trans. Med. Imaging* **2011**, *30*, 22–27. [CrossRef] [PubMed]
175. Hu, L.; Hockett, F.D.; Chen, J.; Zhang, L.; Caruthers, S.D.; Lanza, G.M.; Wickline, S.A. A generalized strategy for designing ^{19}F/^{1}H dual-frequency MRI coil for small animal imaging at 4.7 Tesla. *J. Magn. Reson. Imaging* **2011**, *34*, 245–252. [CrossRef] [PubMed]
176. Schanne, F.A.; Dowd, T.L.; Gupta, R.K.; Rosen, J.F. Development of ^{19}F NMR for measurement of [Ca^{2+}]i and [Pb^{2+}]i in cultured osteoblastic bone cells. *Environ. Health Perspect.* **1990**, *84*, 99–106. [CrossRef] [PubMed]
177. Bar-Shir, A.; Gilad, A.A.; Chan, K.W.Y.; Liu, G.; van Zijl, P.C.M.; Bulte, J.W.M.; McMahon, M.T. Metal ion sensing using ion chemical exchange saturation transfer ^{19}F MRI. *J. Am. Chem. Soc.* **2013**, *135*, 12164–12167. [CrossRef] [PubMed]
178. Bar-Shir, A.; Yadav, N.N.; Gilad, A.A.; van Zijl, P.C.M.; McMahon, M.T.; Bulte, J.W.M. Single ^{19}F probe for simultaneous detection of multiple metal ions using miCEST MRI. *J. Am. Chem. Soc.* **2015**, *137*, 78–81. [CrossRef] [PubMed]
179. Jianxin, Y.; Zhenyi, M.; Yingming, L.; Kenneth, S.K.; Li, L.; Ralph, P.M. Synthesis and evaluation of a novel gene reporter molecule: Detection of b-galactosidase activity using 19F NMR of a fluorinated vitamin B6 conjugate+. *Med. Chem.* **2005**, *1*, 255–262.

180. Kodibagkar, V.D.; Yu, J.; Liu, L.; Hetherington, H.P.; Mason, R.P. Imaging β-galactosidase activity using 19F chemical shift imaging of *LacZ* gene-reporter molecule 2-fluoro-4-nitrophenol-β-D-galactopyranoside. *Magn. Reson. Imaging* **2006**, *24*, 959–962. [CrossRef]
181. Yu, J.; Liu, L.; Kodibagkar, V.D.; Cui, W.; Mason, R.P. Synthesis and evaluation of novel enhanced gene reporter molecules: Detection of β-galactosidase activity using ^{19}F NMR of trifluoromethylated aryl β-D-galactopyranosides. *Bioorg. Med. Chem.* **2006**, *14*, 326–333. [CrossRef] [PubMed]